Current-driven dynamics in molecular-scale devices

2003 J. Phys.: Condens. Matter 15 R521

(http://iopscience.iop.org/0953-8984/15/14/201)

INSTITUTE OF PHYSICS PUBLISHING JOURNAL OF PHYSICS: CONDENSED MATTER

J. Phys.: Condens. Matter **15** (2003) R521–R549 PII: S0953-8984(03)33788-9

TOPICAL REVIEW

Current-driven dynamics in molecular-scale devices

Tamar Seideman

Department of Chemistry, Northwestern University, 2145 Sheridan Road, Evanston, IL 60208-3113, USA

E-mail: seideman@chem.northwestern.edu

Received 6 September 2002
Published 31 March 2003
Online at stacks.iop.org/JPhysCM/15/R521

Abstract

We review recent theoretical work on current-triggered processes in molecular-scale devices—a field at the interface between solid state physics and chemical dynamics with potential applications in diverse areas, including artificial molecular machines, unimolecular transport, surface nanochemistry and nanolithography.

The qualitative physics underlying current-triggered dynamics is first discussed and placed in context with several well-studied phenomena with which it shares aspects. A theory for modelling these dynamics is next formulated within a time-dependent scattering approach. Our end result provides useful insight into the system properties that determine the reaction outcome as well as a computationally convenient framework for numerical realization. The theory is applied to study single-molecule surface reactions induced by a scanning tunnelling microscope and current-triggered dynamics in single-molecule transistors. We close with a discussion of several potential applications of current-induced dynamics in molecular devices and several opportunities for future research.

Contents

1. Introduction

Considerable theoretical effort has been devoted in recent years to the problem of molecular-scale electronics [1, 2]. This effort [3–54] has been fueled by the fascinating physics of conductance at the molecular level, by the anticipation for technological applications, and by laboratory measurements of transport through a variety of imaginative molecular heterojunctions [55–104], including metal–monolayer–metal devices [56, 58, 60, 63, 65–69, 76–79, 84, 85, 87–89, 91, 94, 97–100], molecules assembled onto break junctions [57, 96, 104], single molecules confined between a substrate and a tip [70–74, 93, 102] and conducting molecules isolated in insulating monolayers [55, 64, 101]. The combination of theoretical and numerical work in this area has yielded substantial insights into the response of the conductivity to a variety of general attributes [3–27], including the nature of the molecule–electrode interface [6, 26, 27], the length [12] and chemical structure [13] of the molecular moiety, electron–phonon coupling [15–18], temperature and Coulomb repulsion [22–24]. Recent numerical work provided, in addition, quantitative predictions of the conductance of several specific systems [32–51], including carbon–atom [32, 34, 45] and metal–atom [48, 50, 51] chains, carbon nanotubes [33, 38, 44, 49], fullerenes [43, 46, 47] and a variety of organic molecules [39–42, 50, 51].

A problem of significant fundamental interest, which may also carry practical benefits, and which is only starting to be explored, is the effect of the current on the molecule. Recent theoretical work [105, 106], supported by indirect experimental evidence, suggests that inelastic tunnelling via molecular-scale devices can induce a variety of dynamical processes in molecular heterojunctions. These include vibration, rotation, intermode energy flow and reaction. Potential applications of current-induced dynamics, discussed in detail below, range from new forms of molecular machines and approaches to enhancing the conductivity of molecular wires, to new directions in nanochemistry and nanolithography. Understanding the molecular properties that encourage current-triggered dynamics is relevant also to the design of devices that would be guaranteed to be stable under current.

Interestingly, it is found that molecular wires are highly immune to the strong electric fields that can be generated in the molecular device environment. Density functional calculations for a benzene-1, 4-dithiol molecule attached between two gold electrodes found very minor structural changes at fields as high as 5×10^7 V cm^{-1} [41, 42] (see also [20]). The conversion of a significant amount of electronic energy into vibrational excitation, that underlies current-triggered dynamics, relies on *resonance* tunnelling [105–109].

Resonances are ubiquitous in molecular heterojunctions because systems of relevance are typically conjugated molecules, these being good conductors [4, 10]. Furthermore, the types of molecules widely used in molecular electronics support resonances close to the Fermi level [43, 46, 106], thus offering the opportunity of inducing dynamical events under benign voltage and current conditions. The finite lifetimes of these resonances, mostly due to electron–hole interactions, is controllable to a large extent through functional group substitutions, but is generally short; a few to a few tens of femtoseconds. Often, however, the initial and resonant states are displaced in equilibrium configuration. In that case the electron tunnelling event produces a nonstationary superposition in the resonant state, which evolves during the resonance lifetime. Upon electronic relaxation the system is internally excited and interesting dynamics is likely to ensue [105–109].

The qualitative physics underlying resonance inelastic conductance in molecular devices is quite general. Similar phenomena of nuclear dynamics induced by a transient electronic excitation (an 'electronic kick') take place in a broad variety of experiments, including gas phase electron–molecule scattering [110], photochemistry on conducting surfaces [111, 112] and electron emission surface spectroscopies [113]. An insightful discussion of several such scenarios is provided in an early article by Gadzuk [114]. Below we suggest that the same physics is responsible for the oxidative cleavage of DNA via hole hopping, a problem that has been the focus of intensive experimental and theoretical interest in recent years [115].

The essential parameters determining the outcome of the transient electronic excitation are the timescale of motion in the resonant state relative to the electronic relaxation time, the timescale of dynamics in the ground state relative to the internal relaxation time and the sense of equilibrium displacement between the two states. The molecular device environment offers the possibility of controlling these parameters, and hence the ensuing dynamics.

In the present paper we review recent theoretical and numerical work on the problem of current-induced dynamics in molecular-scale devices. In section 2 we outline the theory [105] and discuss its physical interpretation. In section 3 we present several applications of the formalism of section 2. These include surface reactions induced by the resonant current of a scanning tunnelling microscope (STM) and mechanical motion in single-molecule transistors. In the final section we propose potential applications of current-triggered dynamics and conclude with a discussion of avenues for future research.

2. Theory and interpretation

We consider nuclear dynamics that is triggered by an inelastic, resonance-mediated tunnelling event. In the tip–adsorbate–substrate environment, this would be a surface reaction induced by electron transfer from the tip to the surface or vice versa via an adsorbate-derived resonance. Here electron transfer from the tip to the surface takes place at positive sample bias voltages and is mediated by empty orbitals (orbitals lying above the substrate Fermi level). Electron transfer from the surface to the tip, or equivalently a hole scattering event, takes place at negative sample bias voltages and is mediated by occupied orbitals (orbitals lying below the substrate Fermi level). In the molecular wire environment, we envision directed motion of the molecular moiety, induced by tunnelling from one electrode to the other via a resonance of the molecule + electrodes Hamiltonian, as modified by the bias voltage and possibly a capacitatively connected gate voltage. Formally the two problems are equivalent and can be studied within the same theoretical framework, as outlined below. Numerically and experimentally they differ substantially, and each environment offers different potential applications (*vide infra*).

The complete Hamiltonian is written as

$$H = H_e + H_N + H_{e-N} \tag{1}$$

where H_e describes the electronic dynamics and allows for hopping of electrons between the two electrodes via the adsorbate orbital, H_N is a system-specific nuclear Hamiltonian (see section 3 for examples) and H_{e-N} is the nonadiabatic interaction coupling the electronic and vibrational motions. It is convenient to expand the Hamiltonian in eigenstates of H_e, such that coupling between the extended electronic states of the two electrodes and the discrete state localized on the adsorbate is taken into account nonperturbatively. In this representation

$$H_e = \sum_{\nu} \epsilon_\nu c_\nu^\dagger c_\nu + \sum_{\mu} \epsilon_\mu c_\mu^\dagger c_\mu, \tag{2}$$

where $|\nu\rangle$ and $|\mu\rangle$ are stationary electronic states on the two electrodes and ϵ_ν and ϵ_μ are the

corresponding one-electron energies. The coupling is written in the H_e representation as

$$H_{e-N} = h_N(\boldsymbol{Q}) \sum_{\mu,\nu} (\langle \mu|r\rangle\langle r|\nu\rangle c_\mu^\dagger c_\nu - \langle n_r\rangle), \tag{3}$$

where $\boldsymbol{Q}$ denotes collectively the nuclear coordinates, $|r\rangle$ is the resonant orbital and $\langle n_r\rangle$ denotes its equilibrium occupancy. Equation (3) adapts the coupling term used in studies of vibrational excitation of a linearly coupled harmonic oscillator [116–118] to the problem considered here by replacing the linear dependence on the vibrational coordinate with a general function $h_N(\boldsymbol{Q})$. It is important to point out that equation (1) neglects the dependence of the coupling between the discrete electronic state and the electronic continua on nuclear coordinates. The range of validity of this approximation is discussed below.

Assuming that the nonadiabatic interaction can be described within first-order perturbation theory, we express the reaction rate w as

$$w = 2\frac{2\pi}{\hbar} \sum_{\mu,\nu} \sum_{v_\epsilon} f_i(\epsilon_\nu)[1 - f_f(\epsilon_\mu)]|\langle v_\epsilon, \mu|H_{e-N}|v_0, \nu\rangle|^2 \delta(\epsilon_\nu - \epsilon - \epsilon_\mu), \tag{4}$$

where $|v_0, \nu\rangle = |v_0\rangle|\nu\rangle$, $|v_\epsilon, \mu\rangle = |v_\epsilon\rangle|\mu\rangle$, $|v_0\rangle$ is the initial vibrational state, a bound eigenstate of the nuclear Hamiltonian, and $|v_\epsilon\rangle$ is a final, bound or free eigenstate of the same Hamiltonian. We denote by ϵ the energy transferred from electronic into vibrational, $\epsilon = \epsilon_\nu - \epsilon_\mu$, and the subscript ϵ to v_ϵ serves as a reminder that the energy of the final state is restricted through energy conservation to ϵ above the initial state energy. In equation (4), v_0 denotes collectively the set of quantum indices required to fully specify the parent state. In the case of a bound–bound process in the nuclear mode (such as intermode energy flow, rotational or vibrational excitation or a surface exchange reaction), v_ϵ has a similar significance. In the case of a bound–free reaction in the nuclear modes (such as a desorption or a dissociation), v_ϵ denotes the scattering energy and the quantum indices specifying the internal state of the free product. In the latter case the v_ϵ summation in equation (4) implies summation over the discrete indices and integration over the energy. The factor of 2 in the prefactor of equation (4) accounts for spin degeneracy and $f_{i(f)}(E)$ is a Fermi–Dirac distribution function for electronic states of energy E:

$$f_{i(f)}(E) = 1/\{1 + \exp[(E - E_F^{i(f)})/k_B T]\},$$

where $E_F^{i(f)}$ is the Fermi level of the electrode from (to) which electrons are transferred.

The assumption of $\boldsymbol{Q}$ independence of H_e allows us to reduce equation (4) to a form that provides better insight and is substantially easier to handle numerically. To that end we first separate the vibronic matrix element in equation (4) into inter-dependent electronic and nuclear factors and introduce a complete set of eigenstates of the ground nuclear Hamiltonian:

$$I = \sum_v |v\rangle\langle v| + \sum_n \int \mathrm{d}\epsilon\, |\epsilon n^-\rangle\langle \epsilon n^-|, \tag{5}$$

where $|v\rangle$ are bound and $|\epsilon n^-\rangle$ are incoming wave scattering states of H_N. The collective index v denotes the bound state vibrational indices and n specifies the internal quantum numbers of the free state. With equations (3) and (5) the transition matrix element in equation (4) assumes the form

$$\begin{aligned}\langle v_\epsilon, \mu|H_{e-N}|v_0, \nu\rangle &= \langle \mu|r\rangle\langle r|\nu\rangle\langle v_\epsilon| \left\{ \sum_v |v\rangle\langle v| + \sum_n \int \mathrm{d}\epsilon\, |\epsilon n^-\rangle\langle \epsilon n^-| \right\} h_N(\boldsymbol{Q})|v_0\rangle \\ &\equiv \langle \mu|r\rangle\langle r|\nu\rangle\langle v_\epsilon|\Psi\rangle \end{aligned} \tag{6}$$

where we denote by $|\Psi\rangle$ a superposition of eigenstates of H_N:

$$|\Psi\rangle = \sum_v A_v|v\rangle + \sum_n \int \mathrm{d}\epsilon\, A(\epsilon n)|\epsilon n^-\rangle, \tag{7}$$

with expansion coefficients $A_v = \langle v|h_N(\boldsymbol{Q})|v_0\rangle$ and $A(\epsilon n) = \langle \epsilon n^-|h_N(\boldsymbol{Q})|v_0\rangle$, determined by the current-triggered excitation event.

Equations (6) and (7) provide a formal statement of the physical picture drawn schematically in the previous section. The rapid electron (hole) scattering event produces a superposition of internally excited states of the ground electronic Hamiltonian H_N. The discrete state projection of this superposition, the first term on the right-hand side of equation (7), translates into bound state dynamics; vibration, rotation, intermode energy transfer or a surface exchange reaction. The scattering projection of $|\Psi\rangle$ translates into bound–free dynamics, such as desorption or dissociation.

We proceed by first (section 2.1) specializing the discussion to the case of bound–free processes and next (section 2.2) considering the case of bound–bound processes. In section 2.3 we discuss our method of solving for the electronic dynamics and in section 2.4 we focus on the solution of the nuclear problem.

2.1. Bound–free dynamics

In this subsection we provide an explicit expression for the rate of bound–free processes. These processes are of interest predominantly in the context of STM-assisted nanochemistry and nanolithography (see section 3.1); in a molecular device bound–free dynamics would lead to failure. The bound–free problem benefits from the simplification that the final state is a gas phase molecule and does not suffer vibrational relaxation due to interaction with the substrate. In order to relate the expansion coefficients in equation (7) to observable probabilities, we introduce a set of eigenstates of an asymptotic Hamiltonian, $|\epsilon n\rangle$, related to the full scattering states of H_N, $|\epsilon n^-\rangle$, via the Lippmann–Schwinger equation

$$|\epsilon n^-\rangle = |\epsilon n\rangle + G_N V_N |\epsilon n\rangle. \tag{8}$$

In equation (8), G_N is the Green operator corresponding to the Hamiltonian H_N and V_N is the potential energy operator in that Hamiltonian. In terms of the asymptotically observed states equation (7) is written as

$$|\Psi\rangle = \sum_v A_v|v\rangle + \sum_n \int \mathrm{d}\epsilon\, B(\epsilon n)|\epsilon n\rangle, \tag{9}$$

where $B(\epsilon n) = \sum_{n'} \int \mathrm{d}\epsilon' \langle \epsilon n|\epsilon' n'^-\rangle A(\epsilon' n')$ is the amplitude to observe the state $|\epsilon n\rangle$ at asymptotically long time. It is readily shown [119] that the coefficients $B(\epsilon n)$, containing the information of interest, are given in terms of the (assumed known) excitation coefficients $A(\epsilon n)$ as $\boldsymbol{B} = \mathbf{S}_N \boldsymbol{A}$, where $\boldsymbol{B}$ and $\boldsymbol{A}$ are column vectors with components $B(\epsilon n)$ and $A(\epsilon n)$, respectively, and $\mathbf{S}_N$ is the scattering matrix corresponding to the nuclear Hamiltonian H_N.

Here we do not compute the energy-resolved S matrix but rather use the established connection of the stationary and time-dependent scattering theories to solve for the nuclear dynamics in the time domain. As shown in [119],

$$\begin{aligned} |\Psi(t)\rangle &= \sum_v A_v(t)|v\rangle + \sum_n \int \mathrm{d}\epsilon\, A(\epsilon n t)|\epsilon n^-\rangle \\ &= \sum_v A_v(t)|v\rangle + \sum_n \int \mathrm{d}\epsilon\, B(\epsilon n t)|\epsilon n\rangle \end{aligned} \tag{10}$$

with the initial condition $|\Psi(t=0)\rangle = |\Psi\rangle$. The information of interest, $B(\epsilon n) = \lim_{t\to\infty} \mathrm{e}^{\mathrm{i}Et/\hbar} B(\epsilon n t) = \lim_{t\to\infty} \langle \epsilon n|\Psi(t)\rangle$, is determined by propagating the wavepacket on the neutral ground surface to a long time and projecting it onto the $|\epsilon n\rangle$. The initial condition, $|\Psi\rangle$, is determined by the resonance scattering event, as discussed in section 2.4, and contains the information about the resonance state structure and lifetime.

Substituting equations (6) and (9) in (4), we express the bound–free reaction rate as

$$w(V_b;\tau) = \int \mathrm{d}\epsilon\, P_{\mathrm{reac}}(\epsilon;\tau) W_{\mathrm{exc}}(\epsilon, V_b;\tau), \tag{11}$$

where

$$P_{\mathrm{reac}}(\epsilon;\tau) = \sum_n |B(\epsilon n)|^2 = \sum_n \left| \lim_{t\to\infty} \langle \epsilon n|\Psi(t)\rangle \right|^2, \tag{12}$$

$$W_{\mathrm{exc}}(\epsilon, V_b;\tau) = 2\frac{2\pi}{\hbar} \sum_{\mu,\nu} f_i(\epsilon_\nu)[1 - f_f(\epsilon_\mu)]|\langle\mu|r\rangle\langle r|\nu\rangle|^2 \delta(\epsilon_\nu - \epsilon - \epsilon_\mu), \tag{13}$$

and we indicated explicitly the dependence of the rate on the bias voltage V_b and its parametric dependence on the resonance lifetime τ. Equations (11)–(13) formulate the reaction rate in terms of the current that drives the reaction; $W_{\mathrm{exc}}(\epsilon, V_b;\tau)$ is seen to be the resonant component of the transmission rate through the molecular junction, related to the corresponding current as $W_{\mathrm{exc}} = j/e$, e being the electron charge. Thus, the electronic factor in equation (11), $W_{\mathrm{exc}}(\epsilon, V_b;\tau)$, describes the rate of excitation of the resonance while the nuclear factor, $P_{\mathrm{reac}}(\epsilon;\tau)$, is a normalized probability, describing the reaction probability per resonance excitation. Several attributes that are not experimentally observable and allow insight into the dynamics can be extracted from the time evolution of $\Psi(t)$, as discussed in section 3.1.

2.2. Bound–bound dynamics

We proceed to discuss the case of bound–bound dynamics in the nuclear modes, and first distinguish between reactive and nonreactive processes. Reactive processes are potentially of interest in the STM environment, where we envision resonance-mediated reactions serving as a route to nanochemistry. Here the product state is chemically distinct from the reactant. Such processes have not been described numerically as yet, to our knowledge, and their numerical study would be challenging, as it requires exploring a substantial portion of both potential energy surfaces involved. One of several motivations for numerical investment in this area is the expectation that the chlorination reaction observed experimentally in [120] takes place via the present mechanism. In section 4 we briefly discuss the opportunity of inducing new surface reactions via a STM-triggered, resonance-mediated excitation, with an example from ongoing work.

Nonreactive processes, where the final state is chemically identical to the parent state, are of potential interest in both tip–adsorbate–substrate and molecular device environments. In the former environment, current induced vibrational excitation is already being used in the context of vibrationally inelastic tunnelling spectroscopy, where it serves as a powerful probe of the structure and identity of adsorbates [121–125]. In the latter environment we envision potential applications such as coherently driven molecular machines and manipulation of the conductivity of molecular wires (see section 4). Nonreactive bound–bound processes accompany in general the bound–free dynamics discussed in the previous subsection and are expected also in instances where the energy transferred from electronic into vibrational is insufficient to bring about a bound–free process. The extent to which such processes can be observed depends on the balance between the driving rate and the rate of internal relaxation and on the mode of observation. Although not detected in total desorption yield measurements [108, 126], they can be characterized with the technique of [121–125, 127–129].

The numerical study of bound–bound dynamics requires a proper account of internal relaxation except in cases where the driving rate can be assumed fast compared to the internal relaxation rate. In the latter case one proceeds along similar lines to those described in the previous subsection, namely the (bound state) wavepacket produced in the course of

the excitation event is propagated subject to the Born–Oppenheimer potential V_N, providing nuclear subspace attributes that need to be weighted by the rate of the charge transfer, $W_{\rm exc}$, that provides the energy required for reaction to take place. The nature of the attributes depends on the process envisioned. The simplest case scenario is that of vibrational excitation in effectively 1D systems, see section 3.2. Here the collective index v in equation (7) reduces to a single quantum number and the rate of excitation of the corresponding state in the course of the resonance scattering event is given via the discretized version of equation (11):

$$w_v(V_b;\tau) = P_v(\tau)W_{\rm exc}(\epsilon_v, V_b;\tau). \tag{14}$$

In equation (14), $P_v(\tau) = A_v$ and $W_{\rm exc}(\epsilon_v, V_b;\tau)$ is given by equation (13). Time-resolved observables, such as the expectation value of a given coordinate in the case of vibrational or rotational excitation, or the expectation value of the energy in a given mode in the case of energy transfer, do not lead to observables but may provide a useful insight, as discussed in section 3.2.

2.3. Electronic dynamics

We proceed to describe the solution of the electronic problem, contained in the excitation function $W_{\rm exc}$. To that end we first express equation (13) in terms of projected densities of states as

$$W_{\rm exc}(\epsilon, V_b;\tau) = 2\frac{2\pi}{\hbar}\int {\rm d}\epsilon_\nu\, f_i(\epsilon_\nu)[1 - f_f(\epsilon_\nu - \epsilon)]\rho_i(\epsilon_\nu)\rho_f(\epsilon_\nu - \epsilon), \tag{15}$$

where

$$\rho_i(E) = \sum_\nu |\langle \nu|r\rangle|^2\delta(E - \epsilon_\nu) \tag{16}$$

is the density of electronic states in the initial state, projected onto the resonance orbital, and an analogous expression holds for the projected density of states (DOS) in the final state, $\rho_f(E)$.

Equations (13) and (15) apply to both the molecular device and the tip–adsorbate–substrate environments, which formally are equivalent. The numerical implementation of equation (15), however, differs in the two environments, as the STM environment allows for several approximations that cannot be invoked in the device environment. We first consider the simpler, former environment. Here, under conditions typical of resonance-mediated manipulation experiments [108, 126, 128–130], the tip is remote from the substrate (by 7 Å in the experiment of [108] and by about 20 Å in that of [126], for instance) and the electric field and field gradient at the surface are negligible. In this situation the tip barely modifies the eigenstates of the substrate–adsorbate complex and a valid approximation is obtained by replacing the densities of states in equation (15) with those of the uncoupled tip and substrate–adsorbate systems.

The DOS of the substrate–adsorbate complex can be generally computed to within acceptable (system-dependent) accuracy [131] with current implementations of density functional theory (DFT). The DOS of the tip depends sensitively on the tip structure. As the latter function is typically unknown (often even the chemical composition of the tip is not known with certainty), one invokes simple models, most commonly a single atom adsorbed on a flat metal slab, a pyramid of atoms, or a single atom adsorbed on a large metal hemisphere. Within these simplified models, the tip DOS can be computed using the same procedure applied to compute the substrate–adsorbate DOS.

To gain insight into the essential features determining the observable it is useful to introduce a hierarchy of simplifying approximations, most of which will be subsequently

relaxed. In the limit of an isolated resonance, the projected DOS of the substrate–adsorbate system takes a Lorentzian form [116, 132]:

$$\rho_s(E) = \frac{\Gamma_s(E)/2\pi}{(E-\epsilon_r)^2 + \Gamma^2(E)/4}, \tag{17}$$

where $\Gamma = \Gamma_s + \Gamma_t = \hbar/\tau$ and $\Gamma_{s(t)}$ is the partial width of the adsorbate level due to interaction with the substrate (tip):

$$\begin{aligned}\Gamma_s(E) &= 2\pi \sum_k |V_{kr}|^2 \delta(E-\epsilon_k) \\ &= 2\pi \rho_s^0(E)|\bar{V}|^2.\end{aligned} \tag{18}$$

In equation (18) $|k\rangle$ are bare substrate eigenstates, ρ_s^0 denotes the corresponding density of electronic states and V_{kr} are the matrix elements transferring electrons between the surface and the adsorbate orbital. The line position, ϵ_r in equation (17), includes an energy-dependent shift, given as the Hilbert transform of Γ [119]. The Breit–Wigner approximation replaces the calculation of the DOS of the substrate–adsorbate complex by calculation of the DOS of the bare substrate, in general it is a much easier task. Clearly, the assumption of an isolated resonance does not always hold. Decay laws other than the pure exponential are explored in [133].

If structure in the energy dependence of the tip DOS is broad with respect to the adsorbate-derived resonance width, replacement of ρ_t by a constant is a reasonable approximation. Since realistic modelling of the tip is usually impossible, this approximation is useful also outside its strict range of validity. Within the Breit–Wigner and constant ρ_t approximations, equation (15) takes the form

$$W_{\rm exc}(\epsilon, V_b; \tau) \propto \begin{cases} \displaystyle\int \mathrm{d}\epsilon_\nu \, f_t(\epsilon_\nu + \epsilon)[1 - f_s(\epsilon_\nu)] \frac{\rho_s^0(\epsilon_\nu)}{(\epsilon_\nu - \epsilon_r)^2 + \Gamma^2/4}, & V_b > 0 \\ \displaystyle\int \mathrm{d}\epsilon_\nu \, f_s(\epsilon_\nu)[1 - f_t(\epsilon_\nu - \epsilon)] \frac{\rho_s^0(\epsilon_\nu)}{(\epsilon_\nu - \epsilon_r)^2 + \Gamma^2/4}, & V_b < 0. \end{cases} \tag{19}$$

At low temperatures the Fermi–Dirac distribution reduces to a step function, $f(E) \to \Theta(E_F - E)$. If, in the energy range of interest, the substrate DOS is broad with respect to the resonance decay rate, the energy dependence of the ρ_s^0 can be neglected and $W_{\rm exc}$ simplifies as

$$W_{\rm exc}(\epsilon, V_b; \tau) \propto \begin{cases} \displaystyle\int_{E_F}^{E_F + eV_b - \epsilon} \frac{\mathrm{d}\epsilon_\nu}{(\epsilon_\nu - \epsilon_r)^2 + \Gamma^2/4}, & V_b > 0 \\ \displaystyle\int_{E_F + eV_b + \epsilon}^{E_F} \frac{\mathrm{d}\epsilon_\nu}{(\epsilon_\nu - \epsilon_r)^2 + \Gamma^2/4}, & V_b < 0, \end{cases} \tag{20}$$

where the dependence of the excitation function on the bias voltage, and its parametric dependence on the lifetime, are explicit on both sides. In this limit the integration over ϵ_ν is readily carried out analytically, giving [105]

$$W_{\rm exc}(\epsilon, V_b; \tau) \propto \begin{cases} \left[\tan^{-1}\left(\dfrac{E_F + eV_b - \epsilon - \epsilon_r}{\Gamma/2}\right) - \tan^{-1}\left(\dfrac{E_F - \epsilon_r}{\Gamma/2}\right)\right], & V_b > 0 \\ \left[\tan^{-1}\left(\dfrac{E_F - \epsilon_r}{\Gamma/2}\right) - \tan^{-1}\left(\dfrac{E_F + eV_b + \epsilon - \epsilon_r}{\Gamma/2}\right)\right], & V_b < 0. \end{cases} \tag{21}$$

The closed form approximation of equation (21) illustrates the physical content of the electronic function in equation (11). By contrast to an electron beam, a STM is a broadband source of electrons, with an energy band of order $e|V_b| - \epsilon$, see equation (20). The excitation function,

$W_{\rm exc}(\epsilon, V_b; \tau)$, measures the fraction of the current that is transferred via the resonance orbital and is hence available for depositing energy into the vibrational system.

The sigmoidal voltage dependence of $W_{\rm exc}$, explicit in equation (21), has thus the same physical origin as the 'staircase' structure observed numerically in current–voltage curves in molecular wires [4, 30], namely the eigenlevel spectrum of the molecule + contacts Hamiltonian. References [4, 30] compute the elastic conductance, whereas $W_{\rm exc}$ is proportional to the inelastic conductance. Nonetheless, the voltage dependence of the two functions contains the same molecular information since it depends only on the eigenlevel structure of the device. It is worth noting that the same physics is responsible for the familiar 'staircase' structure of the cumulative reaction probability in bimolecular reactions [134]. While the former [4] 'staircase' reflects a discrete eigenlevel spectrum coupled to two continua in the electronic mode, the latter [134] reflects a discrete eigenlevel spectrum coupled to two continua in the nuclear modes.

The sigmoidal structure of equation (21) rationalizes the bias dependence reported in several recent resonance-assisted STM manipulation studies [108, 126, 128–130]. Furthermore, the sensitivity of the voltage dependence of the observable to $\tau = \hbar/\Gamma$, equation (21), suggests a possible means of determining the resonance lifetime by fitting parametrized theoretical results to experimental yield versus voltage curves. This opportunity is illustrated in section 3.1.

The calculation of $W_{\rm exc}(\epsilon, V_b; \tau)$ in the case of a molecular device is considerably more demanding. Here the resonance is strongly coupled to both continua, the voltage modifies the eigenpairs of the field-free molecule + contacts Hamiltonian and the system is out of equilibrium. Furthermore, because the electrodes extend from $-\infty$ to $+\infty$, the electronic subspace is subject to open-system boundary conditions. This precludes the use of conventional electronic structure routines that are designed for either periodic systems (as in solid state physics) or finite systems (as in quantum chemistry). Fortunately, the intensive theoretical and numerical effort focused on the calculation of conductivity of molecular wires in recent years has led to the development of *ab initio* methods that are capable of handling the above hurdles and providing quantitative descriptions of the electronic dynamics [32–52]. Although the studies of [32–52] have confined attention to the calculation of elastic conductance, equation (15) suggests that the same numerical input required for the elastic case could be utilized for calculation of the inelastic component sought here. In section 3.2 we describe a study of current-induced dynamics in single-molecule transistors, where a DFT nonequilibrium Green function approach is used in conjunction with equation (15) to compute $W_{\rm exc}(\epsilon, V_b; \tau)$. The reader is referred to [106] for details of the methodology.

2.4. Nuclear dynamics

With the excitation function determined at one of the levels of approximation detailed in section 2.3, we proceed to determine the function $P_{\rm reac}(\epsilon; \tau)$, equation (12), which contains the details of the nuclear dynamics. As in the case of the electronic dynamics, the STM environment offers also for solution of the nuclear problem a simplification that does not obtain in the molecular device environment. Here we utilize the fact that the interaction with the tip hardly modifies the eigenstates of the substrate–adsorbate complex to study the (tip-induced) dynamics of the substrate–adsorbate complex free of external fields. We compute Born–Oppenheimer potential energy surfaces for the substrate–adsorbate system in the two states involved and solve the time-dependent Schrödinger equation subject to these potentials with a wavepacket propagation technique [105–109].

In the limit of an isolated resonance the initial condition in equation (10)—the A_v and $A(\epsilon, n)$ excitation coefficients—is conveniently determined by adaptation of the Menzel–Gomer–Readhead (MGR) model [135], often employed to describe photon-stimulated desorption from metal surfaces [111, 112]. This model approximates the resonant electron scattering event as an instantaneous transition of the initial bound eigenstate to the resonance state, propagation of the nonstationary state produced for a residence time τ_R subject to the resonant state potential energy surface, followed by a second instantaneous transition of the evolved wavepacket to the initial electronic state. The continuous nature of the relaxation process is taken into approximate account within the lifetime averaging model of Gadzuk [136]. In this approximation all observables extracted from the asymptotic wavepacket are averaged over τ_R with an exponential weight factor $(1/\tau)\exp(-\tau_R/\tau)$, $\tau = \hbar/\Gamma$ being the resonance lifetime. The reaction probability of equation (12), for instance, is computed as

$$P_{\text{reac}}(\epsilon; \tau) = \frac{1}{\tau}\int_0^\infty \mathrm{d}\tau_R \, \exp(-\tau_R/\tau) P_{\text{reac}}(\epsilon; \tau_R), \tag{22}$$

where $P_{\text{reac}}(\epsilon; \tau_R)$ is extracted from the asymptotic form of a wavepacket that resided a time τ_R in the resonance state. Similarly, the expectation value of a given coordinate or of the energy in a given mode is obtained as

$$\langle \mathrm{O}(t; \tau)\rangle = \frac{1}{\tau}\int_0^\infty \mathrm{d}\tau_R \, \exp(-\tau_R/\tau)\langle \mathrm{O}(t; \tau_R)\rangle, \qquad \langle \mathrm{O}(t; \tau_R)\rangle = \langle \Psi(t; \tau_R|\mathrm{O}|\Psi(t; \tau_R)\rangle. \tag{23}$$

In case the lifetime is determined semi-empirically, rather than *ab initio*, the dynamical simulation is incorporated in a least squares loop fit to an experimental yield versus voltage curve. Specific examples are given in section 3.1.

In the molecular device environment, the coupling of the resonance to both continua is comparable or equal. Accurate description of the nuclear dynamics in this case would require the construction of Born–Oppenheimer potential energy surfaces for the molecule + contacts Hamiltonian in both states involved, a costly problem even if only one or two modes are treated dynamically. As one's goal is to explore the qualitative physics, rather than to provide an accurate description of a specific system, simplified models may nevertheless be useful. Depending on the system and the process envisioned, the use of a small number of metal atoms to represent the electrodes may be adequate for the purpose of constructing potential energy surfaces for the nuclear modes (although not for computation of W_{exc}). Alternatively, *ab initio* data computed for a molecule attached to a single surface can be made use of. Examples are given below.

3. Applications

In this section we describe several applications of the theory outlined in section 2. We start in section 3.1 with a discussion of STM-triggered reactions. In section 3.2 we turn to the problem of current-induced dynamics in single-molecule transistors.

3.1. STM-triggered nanochemistry

The discussion of section 2 suggests that, in the case of STM-triggered dynamics, numerical effort should focus predominantly on the nuclear factor in equation (11). Here accurate treatment of the electronic dynamics is not practical as the structure of the tip is not known. At the same time, valuable information about these dynamics is contained in the data; equation (21)

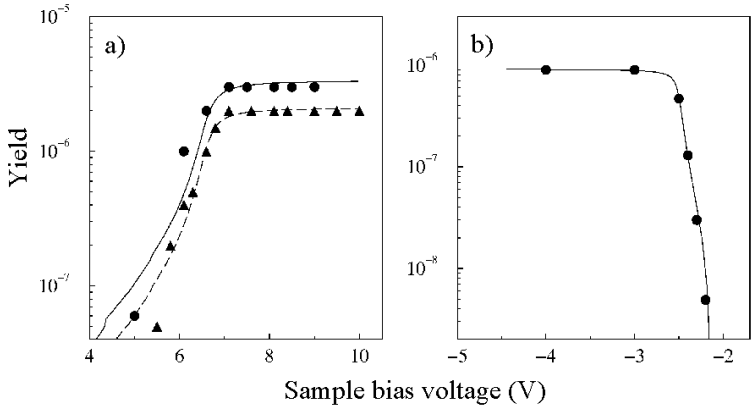

Figure 1. STM-triggered resonance-mediated desorption. (a) Desorption of H-atoms from Si(100)2 × 1:H. The symbols show the experimental data of [126] and the curves show the theoretical results of section 3.1.1. (b) Desorption of C_6H_6 from Si(100). The symbols show the experimental data of [108] and the curves show the theoretical results of section 3.1.2. The error bars are omitted from both sets of experimental data.

and the accompanying discussion illustrate that the voltage dependence of the rate, obtainable in STM experiments [108, 126, 128–130], is strongly dominated by the electronic dynamics. A corollary is that the type of experiments considered here [108, 126, 128–130] provide little insight into the nuclear dynamics. That insight needs to be obtained numerically at the present time. In this subsection we study two STM-induced desorption reactions of complementary nature. We focus on calculation of the nuclear dynamics and employ experimental data to approximate the electronic dynamics.

Two experimental yield versus voltage curves are shown as symbols in figure 1. Panel (a) shows the results of [126] for desorption of H-atoms from hydrogen-passivated Si(100) whereas panel (b) gives the data of [108] for desorption of C_6H_6 from Si(100). (We remark that the reaction yield is proportional to the reaction rate of section 2 and that part of the experimental literature reports the former and part the latter observable.) The two reactions differ substantially in detail but share several features. Both experiments [108, 126] provide evidence for an electronic mechanism; the large tip–surface distance precludes STM manipulation mechanisms that rely on the electric field and field gradient at the surface or on chemical contact. The temperature dependence precludes thermal desorption. The sigmoidal shape of the yield versus voltage curve, predicted by equation (21), is evident in both panels. We remark that these features are common also to the rate versus voltage curves of [128–130], pertaining to the rotation of DCCD on Cu(100) [128], the rotation of CCD on Cu(100) [129] and the displacement of Si adatoms on Si(111)(7 × 7) [130]. An interesting question in connection with figure 1(a) is the lifetime of the underlying resonance, this problem being relevant to H-atom nanolithography [137–140] and the topic of several recent studies. Two remarkable features of figure 1(b) are the sharp voltage dependence and the large yield observed under mild conditions; under comparable conditions about five orders of magnitude lower rates were reported for the STM-triggered resonance-mediated desorption of CO from a copper surface [127]. The former question is addressed in section 3.1.1 and the latter in section 3.1.2.

3.1.1. H-atom desorption from Si(100)2 × 1:H. Electron energy loss spectroscopy of Si(100)2 × 1:H shows a peak with a maximum at 8 eV and an onset at 6 eV [141].

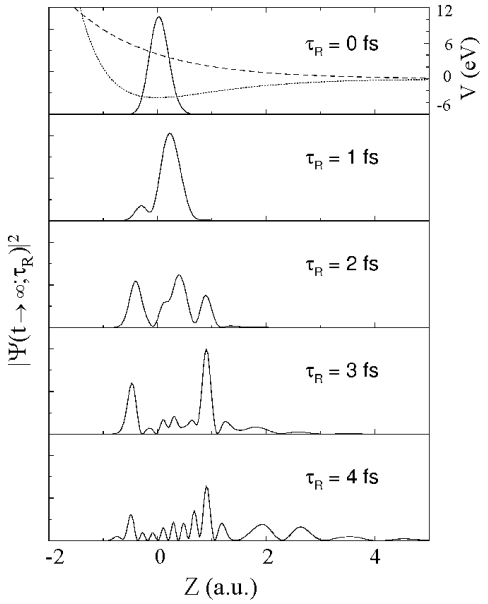

Figure 2. Nuclear dynamics leading to desorption of a H-atom from a silicon surface: asymptotic probability densities for different excited state residence times, τ_R. The ground and excited state potential energy curves of [145] are shown in the top panel. Reproduced with permission from [105].

Calculations [142, 143] identify this feature as the $\sigma \rightarrow \sigma^*$ transition of the Si–H bond, and direct optical excitation experiments with 7.9 eV light [144] confirm this assignment. The experimental results [126], shown as symbols in figure 1(a), provide clear evidence for resonance-mediated desorption, assisted by the excited σ^* state of the H–Si complex.

Potential energy curves for motion perpendicular to the surface in the ground and excited σ^* states of H/Si(100) are constructed in [145] based on *ab initio* electronic structure calculations. These curves are shown as a broken and a dotted curve in the top panel of figure 2. The full curves of figure 2 give the results of our wavepacket simulations subject to the potential energy curves of [145]. Shown is the asymptotic ($t \rightarrow \infty$) ground state probability density versus the distance from the surface, Z, for different excited state residence times, τ_R (see section 2.4). In the trivial case, $\tau_R = 0$, the initial stationary eigenstate is not altered by the resonance tunnelling event and the desorption probability vanishes; conductance is elastic. As τ_R increases, the bound state component of the asymptotic wavepacket has a larger projection onto vibrationaly high states of the H/Si Hamiltonian and an increasing portion of the probability density has been depleted through desorption.

Figure 3 shows the energy-resolved probability, $P_{\text{reac}}(\epsilon; \tau)$ of equation (12), as a function of the electronic-to-vibrational energy transfer, ϵ, and the resonance lifetime, τ. $P_{\text{reac}}(\epsilon; \tau)$ is seen to be a narrowly distributed function of the scattering energy $\epsilon - E_B$ (E_B being the binding energy), peaked about zero. As the lifetime increases, the distribution broadens slightly but throughout the range of lifetimes relevant for the H/Si(100) system (*vide infra*) the desorbate energy distribution remains sharply peaked with a width below 0.3 eV. The implication of figure 3 are discussed below.

Figure 4 illustrates schematically the energetics of the W-tip–Si:H-surface junction. Since the desorption experiments [126, 137, 139, 145] considered here are performed on H-terminated

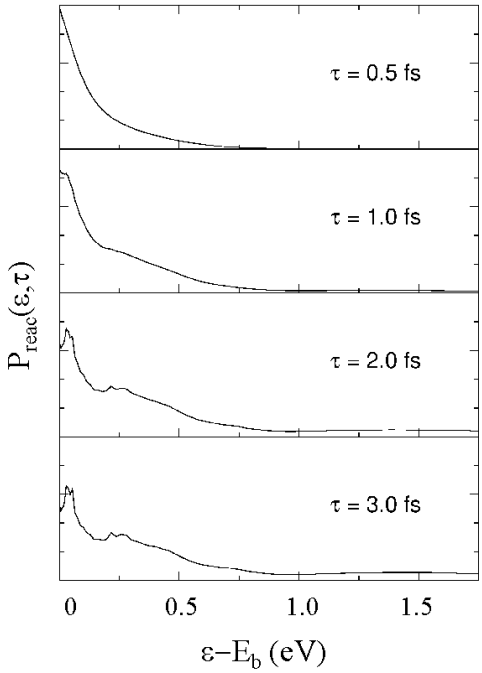

Figure 3. Energy-resolved reaction probabilities, $P_{\mathrm{reac}}(\epsilon;\tau)$ of equation (12), for desorption of H-atoms from Si(100)2 × 1:H as a function of the scattering energy, $\epsilon - E_B$, and the resonance lifetime, τ. Reproduced with permission from [105].

surfaces, the dangling bonds, which significantly affect the DOS of the clean Si(100) surface, do not play a role and ρ_s^0 is better approximated as the density of unoccupied states of bulk silicon than as that of the clean surface. This function, as computed within DFT, is superimposed on the energy scheme of figure 4. Our results agree with a previous calculation of the bulk silicon DOS [146].

The tip DOS was found to have appreciable effect on STM image simulations and conductance spectra [147–152]. The results of [147–152] suggest that other observables of STM experiments may be similarly sensitive to the tip DOS, questioning the validity of the common assumption of constant [116, 117] or free-electron-gas-like [118] DOS and posing a general problem since, as noted in section 2, the tip structure is generally unknown. The sensitivity to the tip DOS is nevertheless system- and observable-dependent. For the case of H-atom desorption from Si(100) induced by a W-tip, we experimented with different models of the tip and did not find appreciable sensitivity of the yield versus voltage curve within reasonable limits. Clearly, this result cannot be extrapolated to other systems and does not apply to extreme cases.

We proceed by using the results of figure 4 for the substrate DOS and setting that of the tip to a constant. The lifetime of the Si–H σ^* state is determined by incorporating the dynamical simulation in a least squares fit loop to the data of [126]. Using equations (11) and (19) we have

$$\text{Yield} = C \int_0^\infty \mathrm{d}\epsilon\, P_{\mathrm{reac}}(\epsilon,\tau) \int_0^{eV_b-\epsilon} \mathrm{d}\epsilon_\nu\, f_t(\epsilon_\nu+\epsilon)[1-f_s(\epsilon_\nu)]\frac{\rho_s^0(\epsilon_\nu)}{(\epsilon_\nu-\epsilon_r)^2+\Gamma^2/4}, \tag{24}$$

where the zero of energy is chosen as the substrate Fermi level E_F. The full curve of figure 1(a)

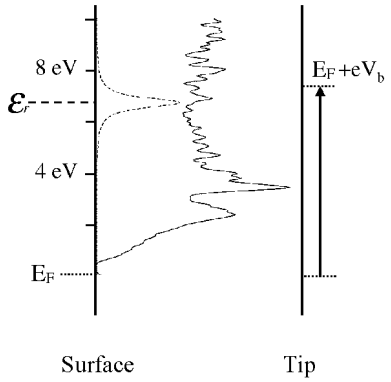

Figure 4. A schematic illustration of the energetics of a W-tip–Si(100):H-surface junction. Superimposed is the electronic DOS of bulk silicon. The position and width of the $\sigma \rightarrow \sigma^*$ resonance, as obtained from a fit of the theoretical results to experimental data (see the text for details) are indicated by the broken curve. We note that the sample work function is 4.91 eV. Reproduced with permission from [105].

gives the numerical desorption yield thus obtained. The lifetime determined is $\tau \approx 1.2$ fs, essentially independent of the substrate temperature.

The H-atom desorption problem is an example of an effectively 1D reaction; excited state motion is along the ground state reaction coordinate, the transient excitation event deposits energy into the reaction mode and intermode energy transfer does not take place. More interesting are multi-dimensional processes, where energy is initially deposited in an internal mode and is subsequently transferred to the reaction mode, due to efficient mode coupling. The latter case is exemplified by the C_6H_6/Si desorption problem, discussed in the next subsection.

3.1.2. C_6H_6 desorption from Si(100). The threshold in the yield versus voltage curve of figure 1(b) coincides to within 0.2–0.3 eV with a sharp peak in the electronic DOS, indicating that a localized state is accessed in the tunnelling event. The peak corresponds to the binding energy of a feature observed in photoemission studies of benzene/Si(100) and attributed to the highest occupied molecular orbital of the adsorption complex [153]. These observations suggest that the STM-triggered desorption is mediated by a positive ion resonance that is predominantly localized on the adsorbate.

Figure 5 illustrates the equilibrium configuration of C_6H_6/Si(100) in the neutral ground state, as obtained from a first principles surface slab calculation [107]. The benzene ring attaches to the Si(100) surface through a Diels–Alder-like [4 + 2] cycloaddition reaction, where the Si dimer acts as a dienophile. Upon adsorption, the aromaticity of C_6H_6 is disrupted, producing a 1, 4-cyclohexadiene-like configuration that is rather strained, due to mismatch of the ring size and the Si–Si dimer distance.

Interestingly, the structure and energetics predicted by the slab calculation are accurately reproduced by a (properly constructed) cluster model. Extensive comparisons of the two types of calculations at various levels of the electronic structure theory are given in [107], where the chemical origin of the good agreement found is clarified. With the validity of a cluster model established, the structure and energy of the stationary state configurations in both neutral and ionic states can be computed with standard quantum chemistry methods in full $3N$-dimensional space, N being the number of adsorbate + cluster atoms. The results of these calculations are superimposed on the contour plots of figure 6.

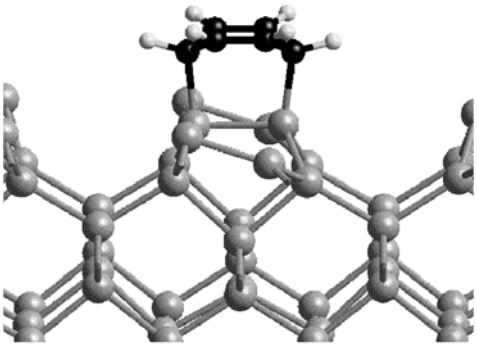

Figure 5. Optimized geometry of the single-dimer-bound configuration of benzene on the Si(100) surface as obtained from a first principles surface calculation. The Si atoms are represented by large grey spheres, the H atoms by small grey spheres and the C atoms by black spheres. Reproduced with permission from [107].

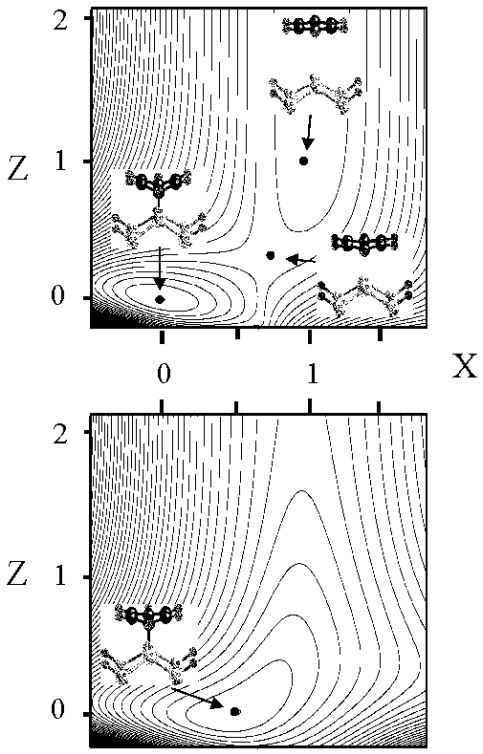

Figure 6. Neutral (a) and ionic (b) potential energy surfaces for C_6H_6/Si(100) versus the dimensionless coordinates of equation (25) as obtained at the B3LYP/6-31G** level. The stationary state configurations on the surfaces are superimposed on the contour plots and their locations are indicated by black dots. Reproduced with permission from [107].

Comparison of the equilibrium configurations of the neutral and cationic forms shows that several geometric modifications accompany ionization of the substrate–adsorbate complex. First, the C–C bonds approach those found in free benzene. Second, the bond angles open up and, third, the Si–C bonds increase in length from 1.97 Å in the neutral state to 2.16 Å in

the ionic state. These data suggest that the STM generates a transient cationic species whose structure differs markedly from that of the neutral state whereas the local C_{2v} symmetry is conserved.

Along with the structures of the stationary states in the neutral surface, depicted in figure 6(a), the ion state equilibrium configuration of figure 6(b) reveals much of the qualitative physics that underlies the desorption process. The neutral state single-dimer-bound configuration is ionized into a cationic state whose equilibrium configuration is significantly displaced with respect to that of the neutral state, primarily along a collective ring-bending mode. The nonstationary state produced is accelerated toward the ionic state minimum, converting potential into kinetic energy of the nuclei. Upon relaxation to the neutral state, the vibrational energy gained, initially deposited for the most part in the ring-bending mode, is rapidly transferred to the desorption mode due to efficient vibrational coupling. With sufficient energy the system surmounts a transition state barrier of about 1.1 eV, after which both Si–C bonds are ruptured in a concerted fashion, leading to desorption. Depending on the kinetic energy gained by the nuclear system in the course of the inelastic resonance tunnelling process, the desorption dynamics may be sensitive to the presence of a shallow physisorption well, whose structure is depicted in the exit valley of figure 6(a).

Reference [107] discusses the physical considerations involved in the construction of an orthogonal coordinate system and the determination of *ab initio* potential energy surfaces for the neutral and ionic states of C_6H_6/Si. We refer the reader to [107] also for the energetics of the stationary states and the functional form of the surfaces, and provide below only a qualitative discussion, assisted by the contour plots of figure 6. Here Z and X are dimensionless coordinates defined as[1]

$$Z = \frac{z - z_{\mathrm{eq}}}{z_{\mathrm{p}} - z_{\mathrm{eq}}}, \qquad X = \frac{(\boldsymbol{Q}' - \boldsymbol{Q}'_{\mathrm{eq}}) \cdot (\boldsymbol{Q}'_{\mathrm{p}} - \boldsymbol{Q}'_{\mathrm{eq}})}{|\boldsymbol{Q}'_{\mathrm{p}} - \boldsymbol{Q}'_{\mathrm{eq}}|^2}, \tag{25}$$

where z is the distance of the centre of mass of the four carbon atoms which are not bound to the silicon surface from the centre of the Si–Si dimer. We express the $3N$ modes of the substrate–adsorbate complex, $\boldsymbol{Q}$, in atomic Cartesian coordinates and define by $\boldsymbol{Q}'$ a vector obtained from $\boldsymbol{Q}$ by subtracting the z coordinates of the adsorbate atoms. The subscripts 'eq' and 'p' refer to the equilibrium and physisorbed configurations, respectively, and we choose the neutral state equilibrium as the origin of the coordinate system and the physisorbed configuration as $Z = X = 1$. Thus, Z takes the role of a desorption coordinate whereas X is a collective mode that accounts for internal motion, predominantly into-plane motion of the carbon backbone, accompanied by relaxation of the silicon dimer.

The potential energy surfaces of figure 6 are next employed to study the nuclear dynamics triggered by the resonance tunnelling process. Figures 7–9 describe the evolution in the neutral state subsequent to the resonance tunnelling event through plots of the expectation values of X and Z in the wavepacket. In figure 7 the initial condition Ψ is determined through $\tau_R = 25$ fs residence in the resonant state. Desorption is initiated by large-amplitude vibrational motion across the chemisorption well. Energy initially deposited in the X mode shuttles periodically between the coupled modes for a brief period, after which the oscillation amplitude of $\langle X \rangle$ decays and desorption is underway, as indicated by the rapid increase of $\langle Z \rangle$. Since a major portion of the wavepacket remains chemisorbed, $\langle X \rangle$ is asymptotically well below the exit valley configuration of $X = 1$. The inset of figure 7 shows a snapshot of the wavepacket at 750 fs, illustrating vibrationally mixed motion in the chemisorption well, some probability density in the physisorption site and a portion of the wavepacket propagating along the exit valley.

[1] In equation (25) we correct a typographic error in equation (2) of [107], where a prime was omitted from $\boldsymbol{Q}$.

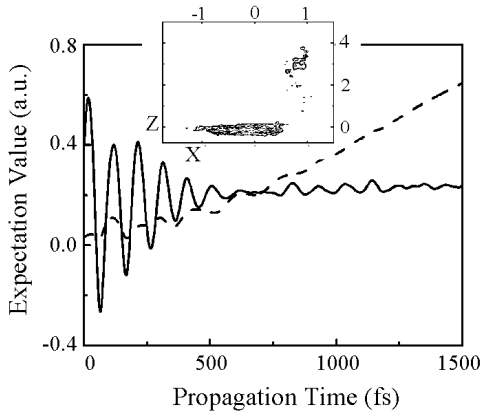

Figure 7. Nuclear dynamics leading to desorption of benzene molecules from a silicon surface: expectation values of X (full curve) and Z (broken curve) in the evolving wavepacket, subsequent to a residence time of 25 fs in the ionic state. The inset shows a snapshot of the wavepacket 750 fs after relaxation, illustrating highly vibrationally mixed motion in the chemisorption well, some probability density in the physisorption site and a portion of the wavepacket propagating along the exit valley. Reproduced with permission from [109].

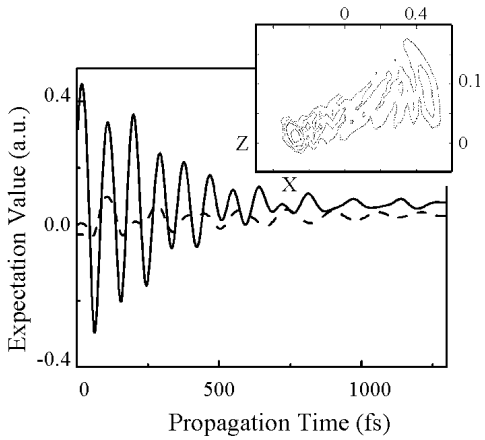

Figure 8. Expectation values of X (full curve) and Z (broken curve) subsequent to a residence time of 20 fs in the ionic state. The inset shows a snapshot of the wavepacket 400 fs after relaxation. The wavepacket undergoes dephasing and revivals and energy is transferred between the two modes but desorption is barely observed. Reproduced with permission from [109].

Figures 8 and 9 contrast the desorption dynamics subsequent to the 25 fs residence time with that following shorter (20 fs) and longer (30 fs) residence times. In the former ($\tau_R = 20$ fs) case the tunnelling event deposits vibrational energy into the nuclear system, giving rise to interesting 'bound-state-like' dynamics as the wavepacket dephases and revives and energy is transferred between the adsorbate modes. Desorption, however, is negligible; the inset of figure 8 shows that 400 fs subsequent to neutralization the wavepacket is localized in the well to within eyeball accuracy. In the latter ($\tau_R = 30$ fs) case the system explores highly repulsive regions of the neutral potential energy surface and hence the amplitude of the short-time vibrational motion in the ring mode is large as compared to the 25 fs counterpart. Within about 50 fs, $\langle Z \rangle(t)$ has evolved past the transition state and by 400 fs the reaction is complete.

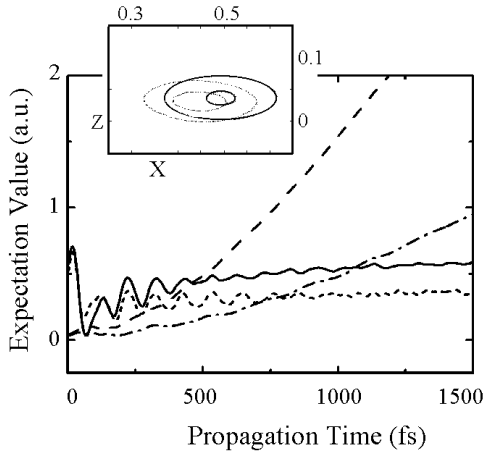

Figure 9. Expectation values of X and Z subsequent to a residence time of 30 fs in the ionic state. The full and broken curves give $\langle X\rangle$ and $\langle Z\rangle$, respectively, in a benzene/Si wavepacket. The dotted and chain curves give $\langle X\rangle$ and $\langle Z\rangle$, respectively, in a staggered p-xylene/Si wavepacket. The inset shows snapshots of the benzene/Si (full contours) and p-xylene/Si (broken contours) at the neutralization instant, $t = 0$. Reproduced with permission from [109].

Functional group substitution provides a chemical handle on the outcome of resonance-mediated reactions. This general feature is exemplified by the dotted and chain curves of figure 9 for the specific case of dimethyl substitution of C_6H_6/Si(100) at the para positions to give p-xylene/Si(100). Elsewhere we illustrate a substantial effect of this substitution (which barely modifies the potential energy surfaces) on the desorption probability. Figure 9 provides only a qualitative illustration of the two mechanisms through which functional group substitutions affect a general resonance-mediated process. A substitution that modifies the reduced mass in the coordinate along which the initial and resonance states are displaced changes the timescale of motion in the resonance state. A substitution that modifies the reduced mass in the reaction coordinate changes the reaction timescale. The former motion competes with electronic relaxation whereas the latter competes with internal relaxation.

The inset of figure 9 compares a p-xylene/Si wavepacket (broken contours) with a benzene/Si wavepacket (full contours) at the neutralization instant. The dotted and broken curves in the main panel show, respectively, the expectation values of X and Z in a p-xylene/Si wavepacket at later times. The small difference in the reduced mass in the X coordinate between the two species allows the heavier one to sample a less repulsive potential upon relaxation, thus decreasing the reaction probability. The difference in the reduced mass in the Z coordinate has no effect on the reaction probability in the limit of infinite internal lifetime (as it does not modify the timescale of motion in the resonance state in this system). Comparison of the broken and chain curves of figure 9 indicates, however, that this difference would have a substantial effect in the presence of internal relaxation.

The time-evolving wavepacket of figures 7–9 is employed to extract the energy-resolved desorption probability using the approach discussed in section 2.4. As was found for the H/Si(100) system in the previous subsection (see figure 3), $P_{\rm reac}(\epsilon;\tau)$ for the C_6H_6/Si(100) desorption is narrowly distributed. The distribution peaks around $\epsilon_0 \approx 1.2$ eV, corresponding to total desorbate energy of $\epsilon_0 - E_B \approx 0.3$ eV. The shift from the resonance energy of the threshold in the yield versus voltage curve predicted by equation (21) is thus roughly 0.3 eV, consistent with observation (figure 1(b)).

The full curve of figure 1(b) gives the results of a numerical fit of equation (11) to the observed yield. Since our fit is based on a small number of data points, and since the experimental error bars are of the order of the data, determination of a definite lifetime is not appropriate but rough upper and lower bounds can be estimated, $7 \lesssim \tau \lesssim 17$ fs. Along with figure 6, the relatively long lifetime of the adsorbate-derived C_6H_6 resonance rationalizes the large yield and the sharp voltage dependence observed for this system.

We remark that the ability of a 2D model to capture the dynamics of the $N = 33$ atom problem is due to features that are specific to the C_6H_6/Si(100) system, in particular the near conservation of C_{2v} symmetry along the reaction pathway. Nonetheless, the fast timescale of the resonance-driven processes envisioned here is expected more generally to restrict the number of active modes to relatively few. Evolution in the resonant state competes with electronic relaxation and is thus of a timescale of femtoseconds. Reaction in the neutral state competes with internal relaxation and is thus of a timescale of sub- to a few picoseconds. On such short timescales, a small portion of the resonance state potential energy surface is explored and, subsequent to electronic relaxation, energy is distributed within a restricted subset of modes.

3.1.3. STM-triggered chemistry: concluding remarks.

(1) The implications of the separation of the coupled vibronic dynamics into an energy integrated product of electronic and nuclear factors, equation (11), are now apparent. The essential approximation in the derivation of equation (11) is the neglect of $\boldsymbol{Q}$ dependence of H_e in equation (1). It follows that the resonance decay rate is independent of the nuclear coordinates. Clearly this approximation is valid if either of two conditions are satisfied. Either the resonance lifetime is short compared to the timescale of nuclear motion on the resonant state potential energy surface, or the motion in the excited state is along an internal mode, rather than along the reaction coordinate. In the former case the wavepacket cannot evolve for a distance long enough in the excited (ionic) state for $W_{\rm exc}$ to change appreciably. In the latter case the decay rate is expected to vary at most slowly as the wavepacket evolves. The first of the above conditions is met in the H-atom desorption problem of section 3.1.1. The second is met in the benzene desorption problem of section 3.1.2. In cases where the lifetime is long compared to the timescale of nuclear motion, and the equilibrium displacement between the initial and resonant states has a substantial component in the reaction mode, equation (11) is not adequate since dependence of the resonance decay rate on the distance from the surface is expected to be roughly exponential. Nonetheless, the insight it provides remains useful.

(2) The finding of a narrowly distributed reaction probability for the H- and the C_6H_6-desorption reactions (similar results were found for photon stimulated desorption of NH_3 from the Cu(111) surface [154]) motivates further approximation of equation (11) as a simple product form:

$$w \approx P_{\rm reac}(\epsilon_0; \tau) W_{\rm exc}(\epsilon_0, V_b; \tau), \tag{26}$$

corresponding to the limit where $P_{\rm reac}(\epsilon; \tau)$ approaches $\delta(\epsilon - \epsilon_0) P_{\rm reac}(\epsilon_0; \tau)$. Equation (26) suggests that the voltage dependence of the observable is insensitive to the potential energy surfaces and the nuclear dynamics. It implies also that, in some cases, a *rough* estimate of the resonance lifetime could be obtained from a fit of the measured data to the voltage dependence of $W_{\rm exc}$, bypassing calculation of the nuclear dynamics. Subject to the conditions discussed in section 2.3, the latter function can be estimated analytically. For the case of H-desorption from Si(100) we found, by fitting $W_{\rm exc}(\epsilon = E_B)$ to the data, a lifetime of 1.4 fs, in rough agreement with the result obtained via equation (24).

Essentially the same result is obtained for this reaction when the analytical approximation of $W_{\rm exc}(\epsilon = E_B)$, equation (21), is used. The latter simplification results from the weak energy dependence of the electronic DOS on the scale of the resonance width, see figure 4. A qualitative discussion of several other experimentally observed STM-triggered surface processes within the $P_{\rm reac}(\epsilon) \to P_{\rm reac}(\epsilon_0)\delta(\epsilon - \epsilon_0)$ limit of equation (26) is given in [105].

(3) It is important to note the differences between the problem of H-atom desorption from Si(100)2 × 1:H, discussed in section 3.1.1, and the problem of benzene desorption from Si(100), discussed in section 3.1.2. The former is triggered by an inelastic electron scattering event that transiently populates an electronically excited state. The latter involves transient formation of a charged species. In addition, the former problem is mediated by a repulsive excited state, hence desorption could in principle take place also in the excited state, while in the latter the ionic state is bound. Finally, the former reaction involves field-emitted, while the latter involves tunnelling, electrons. From the formal viewpoint, however, these problems are similar and both can be accommodated within the framework developed in section 2.

3.2. Current-triggered dynamics in single-molecule transistors

In this section we apply the theory of section 2 to a particularly simple problem, namely current-induced vibrational excitation of a fullerene adsorbed between two gold contacts. Our choice of a simplest-case-scenario model has several motivations. The first is a recent experiment by Park *et al* [155], which records the signature of current-induced vibrational motion in single Au–C_{60}–Au transistors. We are not aware of previous experimental demonstrations of current-induced dynamics in a molecular device, although we believe that the concept is general. Second, the Au–C_{60}–Au system offers rich and relatively well-understood [106] electronic dynamics. The ability to control the electronic dynamics, already demonstrated for this system [106, 155], provides potentially a route of manipulating also the nuclear dynamics (*vide infra*). Third, the nuclear dynamics allows for an analytical approximation which provides useful insight.

The molecular device in mind is depicted in figure 10. The Au electrodes extend to electron reservoirs at $z = \pm\infty$, where bias voltage V_b is applied and electric current is collected. A metal gate with gate voltage V_g is placed near the C_{60} molecule, providing a third probe capacitively coupled to the C_{60}. In figure 11 we describe the electronic dynamics of the device of figure 10, as computed within a DFT-based nonequilibrium Green function approach [106]. The inset shows the computed transmission, $T(E, V_b, V_g)$, versus the electron energy, E, at zero bias and gate voltage. The energy scale is set such that $E_F = 0$. $T(E, V_b, V_g)$ is sharply peaked about $E \sim 0.15$ eV, with a lineshape close to the Breit–Wigner form, indicating an isolated resonance and essentially energy-independent direct transmission. This resonance is responsible for the nuclear dynamics. For reference below, we note that its width corresponds to a resonance lifetime of about 26 fs. At finite bias voltages, $V_b \neq 0$, the eigenlevels, and with them the transmission peaks, shift significantly but the overall shape of $T(E, V_b, V_g)$ is only slightly modified. The effect of a finite gate voltage on the transport properties is rather more substantial. By changing the charge distribution in the molecular region and shifting the energy levels, a nonzero gate voltage alters qualitatively both the line-centre and the shape of the transmission curve [106].

The main part of figure 11 shows the excitation function, $W_{\rm exc}(\epsilon, V_b; \tau)$ of equation (15), versus the electronic-to-vibrational energy transfer, ϵ, and the bias voltage, V_b. We find that

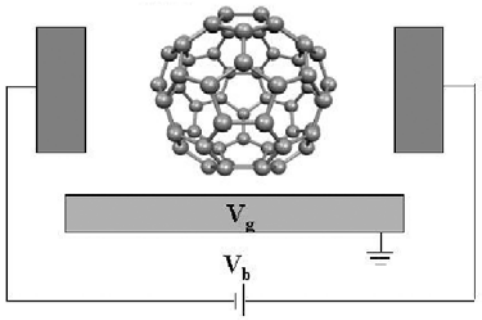

Figure 10. Current-triggered dynamics in single-molecule transistors. Schematic diagram of the Au–C_{60}–Au molecular device. The Au electrodes extend to $z = \pm\infty$ where bias voltage V_b is applied. A gate voltage V_g may be applied at the scattering region of the device.

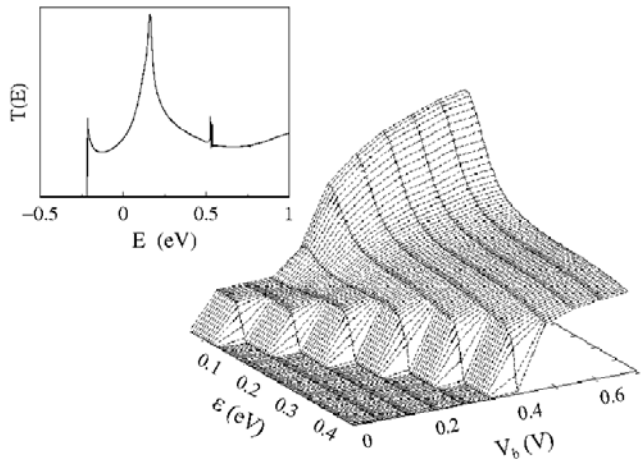

Figure 11. Electronic dynamics in the Au–C_{60}–Au device of figure 10 as obtained within a DFT-based nonequilibrium Green function approach. The main panel shows the excitation function W_{exc} of equation (15) versus the electronic-to-vibrational energy transfer, ϵ, and the bias voltage, V_b. The inset gives the transmission coefficient, $T(E, V_b, V_g)$, versus energy, E, for zero bias and gate voltages. The transmission peak arises from the resonant orbital that mediates the current-triggered dynamics of figure 12.

the excitation function determined *ab initio* for a voltage-biased molecular transistor follows nicely the form of the analytical approximation derived in section 2.3 [105], namely a sigmoidal function of voltage and energy.

The nuclear dynamics triggered by the electronic transmission of figure 11 is similar in concept to the STM-triggered dynamics of section 3.1. The tunnelling event transiently places the nuclear system in a negative ion state of the Au–C_{60}–Au system. Due to the equilibrium mismatch between the neutral and ionic states, a nonstationary superposition of vibrational eigenstates is formed, which travels toward the ionic state equilibrium while continuously relaxing to the neutral state. Upon electronic relaxation the population has been redistributed between the vibrational levels of the neutral surface—the fullerene bounces between the gold contacts until vibrational relaxation returns the system to the ground vibrational state.

In the harmonic limit these dynamics are readily solved analytically. We expand the nonstationary superposition evolving on the ionic surface as

$$\psi(t,z) = \mathrm{e}^{-\mathrm{i}\omega t/2}\sum_v C_v u_v(z-\delta z_{\mathrm{eq}})\mathrm{e}^{-\mathrm{i}v\omega t}, \tag{27}$$

where z denotes distance from the surface, measured with respect to the neutral state equilibrium configuration, δz_{eq} is the equilibrium displacement of the ionic state with respect to the neutral state, ω is the vibrational frequency, assumed equal in the two states, u_v are harmonic oscillator functions and

$$\begin{aligned} C_v &= \langle u_0(z)|u_v(z-\delta z_{\mathrm{eq}})\rangle \\ &= \frac{\zeta_{\mathrm{eq}}^v \exp(-\zeta_{\mathrm{eq}}^2/4)}{\sqrt{2^v v!}}, \qquad \zeta_{\mathrm{eq}} \equiv \sqrt{\mu\omega}\delta z_{\mathrm{eq}}, \end{aligned} \tag{28}$$

μ being the mass. Substituting equation (28) in (27) we have that the probability density in the resonance state oscillates without change of shape about the ionic state equilibrium configuration with amplitude δz_{eq} and frequency ω:

$$|\psi(t,z)|^2 = \sqrt{\frac{\mu\omega}{\pi}}\mathrm{e}^{-(\zeta-\zeta_{\mathrm{eq}}\cos\omega t)^2}, \qquad \zeta \equiv \sqrt{\mu\omega}z. \tag{29}$$

In the harmonic limit the probability of excitation of the vth vibrational level of the neutral state upon electronic relaxation is

$$P_v(\tau_R) = \left|\sum_{v'} C_{v'}\langle u_v(z)|u_{v'}(z-\delta z_{\mathrm{eq}})\rangle \mathrm{e}^{-\mathrm{i}v'\omega\tau_R}\right|^2. \tag{30}$$

In particular, the probability of capture into the ground vibrational level is

$$\begin{aligned} P_0(\tau_R) &= \left|\sum_v \frac{\zeta_{\mathrm{eq}}^{2v}\exp(-\zeta_{\mathrm{eq}}^2/2)}{2^v v!}\mathrm{e}^{-\mathrm{i}v\omega\tau_R}\right|^2 \\ &= \mathrm{e}^{-\zeta_{\mathrm{eq}}^2[1-\cos(\omega\tau_R)]}. \end{aligned} \tag{31}$$

As expected, vibrational excitation, $\sum_{v\neq 0} P_v$, vanishes and elastic conductance ensues in the limit of small equilibrium displacement; $P_0(\tau_R, \delta z_{\mathrm{eq}} \to 0) \to 1$, and in the limit of short residence time in the ionic state; $P_0(\tau_R \to 0, \delta z_{\mathrm{eq}}) \to 1$.

Considering next the vibrational dynamics of the Au–C_{60}–Au device, we adopt the potential energy surfaces given in [155] based on electronic structure calculation [156] of the C_{60}/Au(110) system. A relatively small equilibrium displacement, 4 pm, is predicted by the calculation of [156] and used in the dynamical simulations illustrated below. For generality, we comment also on the numerically observed effect of varying this parameter.

The inset of figure 12 shows the probability of capture into the lowest five vibrational levels as a function of τ_R. The long τ_R behaviour of the $P_v(\tau_R)$ is given for pedagogical completeness; only the small τ_R edge of the figure is of physical relevance since, for the lifetime of the resonance in question (figure 11, inset), τ_R values beyond ≈450 fs do not contribute to the lifetime averaged result of equation (22). $P_0(\tau_R)$ (full curve) follows closely the structure predicted by equation (31) although, due to the anharmonicity of the potential, the periodicity of equation (31) is lost and the amplitude of subsequent recurrences decreases slowly with τ_R. As v increases, $P_v(\tau_R)$ broadens and shifts to larger values of τ_R (modulo $2\pi/\omega$), reflecting the spatial location and breadth of the vibrational eigenfunctions of the neutral state Hamiltonian. With increasing equilibrium displacement, δz_{eq}, the $P_v(\tau_R)$ become better localized in time, decaying exponentially to zero between recurrences, as predicted by equation (31).

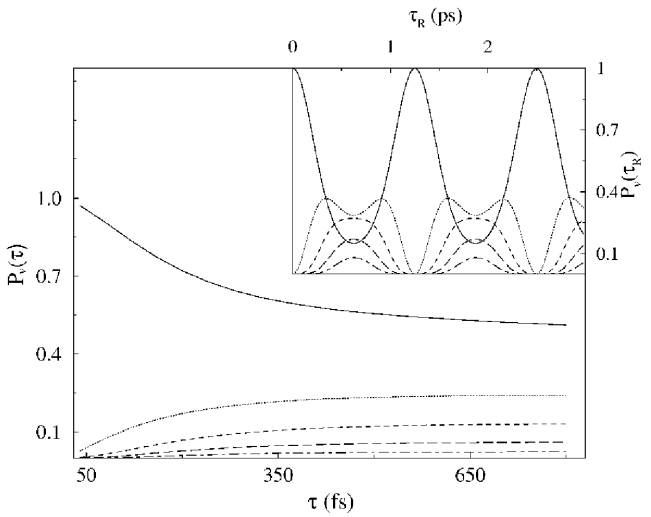

Figure 12. Nuclear dynamics in the Au–C_{60}–Au device of figure 10. Vibrational excitation probabilities $P_v(\tau)$ versus the electronic lifetime, τ, and the vibrational quantum number, v. The equilibrium displacement between the neutral and ionic states is $\delta z_{\rm eq} = 4$ pm. Full curves: $v = 0$, dotted curves: $v = 1$, broken curves: $v = 2$, long-broken curves: $v = 3$, chain curves: $v = 4$. The inset gives the corresponding unaveraged probabilities, $P_v(\tau_R)$ versus the residence time τ_R, see equation (22).

The physical vibrational excitation probabilities, $P_v(\tau)$ of equation (14), are plotted versus τ in the main part of figure 12 for $v = 0, \ldots, 4$. $P_0(\tau)$ decays to a nonzero asymptotic value that decreases with increasing $\delta z_{\rm eq}$. The higher-v probabilities increase monotonically from zero and saturate on a value that depends sensitively on $\delta z_{\rm eq}$. As the equilibrium displacement increases, the vibrational excitation probabilities of progressively higher levels reach a maximum before decaying to the asymptotic plateau. This behaviour follows from equation (22) and the τ_R dependence of the $P_v(\tau_R)$, which becomes smoother with increasing v and with decreasing $\delta z_{\rm eq}$.

The inset of figure 13 shows the expectation value of z in the neutral state wavepacket as obtained through equation (23) with a lifetime of $\tau = 26$ fs, corresponding to the width of the resonance shown in figure 11 (i.e. $\Gamma = \hbar/\tau \approx 0.025$ eV). We find that the C_{60} centre of mass oscillates between the contacts at the fundamental frequency of the neutral surface and an amplitude approximately equal to the distance travelled in the ionic state. Slow damping of the oscillations is due to the anharmonicity of the potential.

The main part of figure 13 shows the vibrational excitation rate of the Au–C_{60}–Au system, $w_v(V_b)$ of equation (14), as a function of the applied voltage V_b for $v = 1$. Our results correspond to the unmodified molecular junction, $V_g = 0$, and are given for $\delta z_{\rm eq}$ values covering the physically relevant range; for smaller $\delta z_{\rm eq}$ the vibrational excitation vanishes (see equation (31) and the discussion below). For larger values we find (within the model potential energy surfaces used [155, 156]) a finite desorption probability. The bias-voltage dependence of the w_v follows the V_b dependence of the $W_{\rm exc}$ in equation (14), see figure 11, and is well approximated by the analytical expression of section 2.3 as a result of the nearly pure Breit–Wigner form of the resonance mediating the dynamics. The excitation rate of vibrational levels $v > 1$, takes a similar shape but responds differently to the magnitude of the equilibrium displacement.

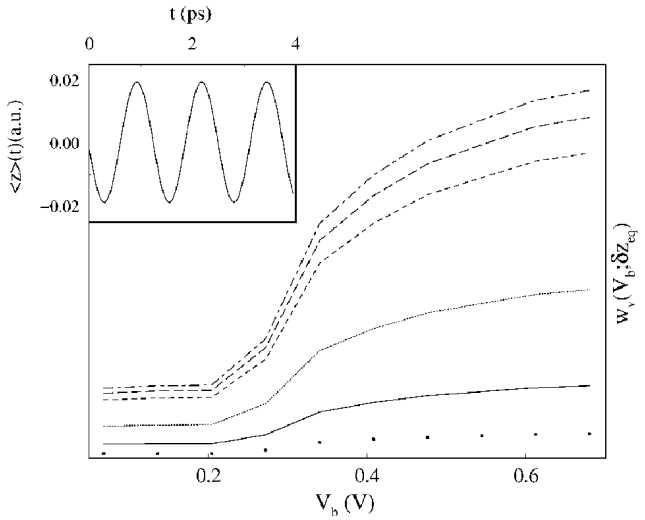

Figure 13. Rate of vibrational excitation of the Au–C_{60}–Au device versus the bias voltage, see equation (14). The equilibrium displacement between the neutral and ionic states is $\delta z_{\rm eq} = 1.24$ pm (circles), 4 pm (full curves), 10 pm (dotted curves), 20 pm (broken curves), 25 pm (long-broken curves) and 31 pm (chain curves). To allow display on the same scale, the $\delta z_{\rm eq} = 1.24$ pm results are multiplied by a factor of 5. The inset shows the expectation value of Z in the wavepacket subsequent to the resonance tunnelling event.

We find that the essential dynamics is contained in the combination of the equilibrium displacement and the resonance lifetime. The former parameter determines the outcome through the exponential dependence of $P_{\rm reac}$ on $\delta z_{\rm eq}$, see equation (31). The latter parameter determines the rate through the balance between the τ dependences of the electronic and nuclear dynamics. Whereas $W_{\rm exc}$ decreases sharply with increasing τ (see equation (21)), $P_{\rm reac}$ increases exponentially with this parameter (see equation (31)). The ability to manipulate the conductance by varying the distance between the electrodes and the gate voltage thereby translates into control of the current-induced dynamics.

4. Summary and outlook

In the previous sections we reviewed recent theoretical work on the problem of single-molecule dynamics induced by electric current, a young and exciting area of research that shares common aspects with several established fields, including transport through molecular wires, photochemistry on conducting surfaces, STM manipulation and electron–molecule scattering.

Subsequent to a discussion of the qualitative physics underlying current-triggered dynamics in section 1, we developed a theoretical framework for study of these dynamics in section 2. By introducing an approximation in the form of the electronic Hamiltonian in equation (1), we converted the solution of correlated reactions in the electronic and nuclear modes, equation (4), into a form that provides better insight and is substantially easier to deal with numerically, equation (11). In the latter form, the reaction rate is expressed in terms of the resonant current that drives the reaction, $j = W_{\rm exc}/e$, and a normalized reaction probability, $P_{\rm reac}$. The parameters determining the dynamics are spelled out and the computational effort is reduced to that required for a conductance calculation and a reaction dynamics calculation in the nuclear subspace. Methods of computing the two inter-dependent functions in equation (11)

were briefly outlined in sections 2.3 and 2.4. An analytical approximation of W_{exc}, section 2.3, rationalizes a common feature of several experiments, namely the sigmoidal shape of the observed rate versus voltage curves.

Application was made to study STM-triggered surface reactions (section 3.1) and current-triggered dynamics in a molecular device (section 3.2). The results of section 2.3 were used to propose the possibility of extracting the electronic dynamics from experimental data. A critical discussion of the approximation leading to equation (11) was given in section 3.1.3.

At present our interest in current-triggered dynamics in molecular scale devices is of fundamental origin. We feel, however, that future work in this area may lead to interesting applications. These may include:

(i) *New forms of molecular machines:* the area of artificial molecular machines [157] has been evolving rapidly for nearly two decades, leading to laboratory-made turnstiles, shuttles, switches and rotors, driven by light, chemistry or electrochemistry [157]. On the one hand, this work exposes the beauty of molecular machines and points to a variety of technological applications. On the other, it reveals the need for a complementary form of molecular machine that could be addressed *individually*, thus eliminating the ensemble average that is inherent to the solution phase.
Current-triggered dynamics in molecular heterojunctions could make a route to that end. We envision using resonance inelastic current to selectively deposit energy in a given mode and hence induce directed motion of the molecular component, see section 3.2. In ongoing work we employ this concept to devise a coherently driven, uni-directional molecular rotor.

(ii) *Implications for conductance calculations:* often in molecular wires the conductivity depends sensitively on the structure of the molecule. An example is the biphenyl family, where the conductance changes by over an order of magnitude with the torsion angle between the rings. In these systems torsion may be expected to ensue resonance tunnelling since the ionic states of biphenyl differ substantially from the ground neutral state in the equilibrium configuration, specifically along the torsion angle. In an ongoing study we show that resonance conductance through a biphenyl molecule attached between metal electrodes gives rise to motion in the torsion angle, and thus conductance enhancement. How general is this result remains to be explored. Current-triggered vibration may likewise modify the conductivity of wires. An experimental study of electron transfer from a metal surface to a molecule [158] finds the electron transfer probability to be greatly enhanced by excitation of the molecule to high vibrational levels. Systems where molecular dynamics hinders the conductance, by driving the system out of the optimal conductance configuration, may likewise be envisioned.

(iii) *Nanochemistry:* an intriguing possibility is that of using an STM tip to induce surface reactions that do not occur spontaneously and study them on a single-molecule, site-specific level. An example that is being addressed in ongoing work is the surface proton transfer reaction, $NH_3/Si \rightarrow NH_2/Si + H/Si$. Also of interest are surface halogenation reactions of the type observed in [120], where the reaction outcome is sensitive to the adsorption site of the parent state.

(iv) *Design criteria:* current-induced dynamics in molecular devices may have undesired consequences; in extreme cases it may lead to failure. The design of current-immune devices relies on understanding the molecular properties that encourage current-triggered dynamics.

(v) *Opportunities in molecule-scale lithography:* nanolithography based on resonance-mediated desorption of H-atoms from Si(100) is an established field with a variety of

applications [126, 138–140]. Organic molecules may offer an interesting complementary route. In the adsorbed state conjugated organics support low energy resonances (lying close to the Fermi level), corresponding to much lower voltages than those used for the H/Si desorption, hence smaller tip–surface separations and enhanced resolution. Further, as discussed in [159, 160], the properties of organic adsorbates can be tuned, via functional group substitution.

Clearly, much remains to be done in the area of current-triggered dynamics in molecular nano-devices. Exploring the above proposed potential applications is one of the topics of ongoing research in our group. Of considerable interest is the development of improved methods for computing the electronic dynamics. As discussed elsewhere [52], approaches that go beyond the current implementation of DFT (such as time-dependent DFT) would be useful also for computation of elastic conductance through frozen molecular wires. For the present application such approaches would be yet more desirable as they would allow the use of electronically excited states to current-induce dynamics in molecular heterojunctions. Another exciting avenue that we hope to address is the development of a method that goes beyond the approximation leading to equation (11) by solving simultaneously for the electronic and nuclear dynamics.

Acknowledgments

The author is grateful to several postdoctoral fellows and colleagues who contributed to the work reviewed in this article or to related experiments; Saman Alavi, Roger Rousseau, Greg Lopinski, Robert Wolkow and Hong Guo. This work was partially supported by the Natural Science and Engineering Research Council of Canada.

References

[1] Ratner M A and Jortner J (ed) 1997 *Molecular Electronics* (Oxford: Blackwell) p 5
[2] Aviram A and Ratner M (ed) 1998 *Molecular Electronics: Science and Technology* (New York: New York Academy of Sciences)
[3] Mujica V, Kemp M and Ratner M A 1994 *J. Chem. Phys.* **101** 6849
[4] Mujica V, Kemp M, Roitberg A and Ratner M A 1996 *J. Chem. Phys.* **104** 7296
[5] Yaliraki S N, Roitberg A E, Gonzalez C and Ratner M A 1999 *J. Chem. Phys.* **111** 6997
[6] Yaliraki S N, Kemp M and Ratner M A 1999 *J. Am. Chem. Soc.* **121** 3428
[7] Mujica V, Roitberg A E and Ratner M A 2000 *J. Chem. Phys.* **112** 6834
[8] Samanta M P, Tian W, Datta S, Henderson J I and Kubiak C P 1996 *Phys. Rev.* B **53** R7626
[9] Datta S, Tian W, Hong S, Reifenberger R, Henderson J J and Kubiak C P 1997 *Phys. Rev. Lett.* **79** 2530
[10] Tian W, Datta S, Hong S, Reifenberger R, Henderson J I and Kubiak C P 1997 *Physica* E **1** 304
[11] Tian W, Datta S, Hong S, Reifenberger R, Henderson J J and Kubiak C P 1998 *J. Chem. Phys.* **109** 2874
[12] Joachim C and Vinuesa J F 1996 *Europhys. Lett.* **33** 635
[13] Magoga M and Joachim C 1997 *Phys. Rev.* B **56** 4722
[14] Joachim C and Magoga M 2002 *Chem. Phys.* **281** 347
[15] Ness H and Fisher A J 1999 *Phys. Rev. Lett.* **83** 452
[16] Dash L K and Fisher A J 2001 *J. Phys.: Condens. Matter* **13** 5035
[17] Ness H and Fisher A J 2002 *Europhys. Lett.* **57** 885
[18] Ness H and Fisher A J 2002 *Chem. Phys.* **281** 279
[19] Todorov T N, Briggs G A D and Sutton A P 1993 *J. Phys.: Condens. Matter* **5** 2389
[20] Todorov T N, Hoekstra J and Sutton A P 2000 *Phil. Mag.* B **80** 421
[21] Treboux G 2000 *J. Phys. Chem.* B **104** 9823
[22] Petrov E G and Hänggi P 2001 *Phys. Rev. Lett.* **86** 2862
[23] Petrov E G, Zelinskii Ya R and Hänggi P 2001 *Mol. Cryst. Liq. Cryst.* **361** 209
[24] Lehmann J, Ingold G-L and Hänggi P 2002 *Chem. Phys.* **281** 199

[25] Petrov E G, May V and Hänggi P 2002 *Chem. Phys.* **281** 211
[26] Cuniberti G, Fagas G and Richter K 2002 *Chem. Phys.* **281** 465
[27] Emberley E G and Kirczenow G 1999 *Phys. Rev.* B **60** 6028
[28] Emberly E G and Kirczenow G 2000 *Phys. Rev.* B **62** 10451
[29] Emberly E G and Kirczenow G 2002 *Chem. Phys.* **281** 311
[30] For a review and comparison of several of the above methods see,
Hall L E, Reimers J R, Hush N S and Silverbrook K 2000 *J. Chem. Phys.* **112** 1510
[31] Lang N D 1995 *Phys. Rev.* B **52** 5335
[32] Lang N D and Avouris P 1998 *Phys. Rev. Lett.* **81** 3515
[33] Delaney P, Di Ventra M and Pantelides S T 1999 *Appl. Phys. Lett.* **75** 3787
[34] Lang N D and Avouris Ph 2000 *Phys. Rev. Lett.* **84** 358
[35] Lang N D and Avouris Ph 2000 *Phys. Rev.* B **62** 7325
[36] Di Ventra M, Pantelides S T and Lang N D 2000 *Phys. Rev. Lett.* **84** 979
[37] Di Ventra M, Pantelides S T and Lang N D 2000 *Appl. Phys. Lett.* **76** 3448
[38] Rochefort A, Di Ventra M and Avouris Ph 2001 *Appl. Phys. Lett.* **78** 2521
[39] Di Ventra M, Kim S G, Pantelides S T and Lang N D 2001 *Phys. Rev. Lett.* **86** 288
[40] Lang N D and Avouris Ph 2001 *Phys. Rev.* B **64** 125323
[41] Di Ventra M, Pantelides S T and Lang N D 2002 *Phys. Rev. Lett.* **88** 046801
[42] Di Ventra M, Lang N D and Pantelides S T 2002 *Chem. Phys.* **281** 189
[43] Taylor J, Guo H and Wang J 2001 *Phys. Rev.* B **63** 121104
[44] Taylor J, Guo H and Wang J 2001 *Phys. Rev.* B **63** 245407
[45] Larade B, Taylor J, Mehrez H and Guo H 2001 *Phys. Rev.* B **64** 075420
[46] Larade B, Taylor J, Zheng Q R, Mehrez H, Pomorski P and Guo H 2001 *Phys. Rev.* B **64** 195402
[47] Roland C, Larade B, Taylor J and Guo H 2002 *Phys. Rev.* B **65** 041401
[48] Mehrez H, Wlasenko A, Larade B, Taylor J, Grütter P and Guo H 2002 *Phys. Rev.* B **65** 195419
[49] Kaun C-C, Larade B, Mehrez H, Taylor J and Guo H 2002 *Phys. Rev.* B **65** 205416
[50] Damle P S, Ghosh A W and Datta S 2001 *Phys. Rev.* B **64** 201403R
[51] Damle P S, Ghosh A W and Datta S 2002 *Chem. Phys.* **281** 171
[52] Xue Y, Datta S and Ratner M A 2002 *Chem. Phys.* **281** 151
[53] Hirose K and Tsukada M 1995 *Phys. Rev.* B **51** 5278
[54] For a review that focuses primarily on theoretical work see,
Nitzan A 2001 *Annu. Rev. Phys. Chem.* **52** 681
[55] Bumm L A, Arnold J J, Cygan M T, Dunbar T D, Burgin T P, Jones L, Allara D L, Tour J M and Weiss P S 1996 *Science* **271** 1705
[56] Zhou C, Deshpande M R, Reed M A, Jones L and Tour J M 1997 *Appl. Phys. Lett.* **71** 611
[57] Reed M A, Zhou C, Muller C J, Burgin T P and Tour J M 1997 *Science* **278** 252
[58] Reinerth W A, Jones L II, Burgin T P, Zhou C W, Muller C J, Deshpande M R, Reed M A and Tour J M 1998 *Nanotechnology* **9** 246
[59] Bumm L A, Arnold J J, Dunbar T D, Allara D L and Weiss P S 1999 *J. Phys. Chem.* B **103** 8122
[60] Chen J, Reed M A, Rawlett A M and Tour J M 1999 *Science* **286** 1550
[61] Chen J, Calvet L C, Reed M A, Carr D W, Grubisha D S and Bennet D W 1999 *Chem. Phys. Lett.* **313** 741
[62] For a review see,
Reed M A 1999 *Proc. IEEE* **97** 652
[63] Reed M A, Chen J, Rawlett A M, Price D W and Tour J M 2001 *Appl. Phys. Lett.* **78** 3735
[64] Donhauser Z J, Mantooth B A, Kelly K F, Bumm L A, Monnell J D, Stapleton J J, Price D W Jr, Rawlett A M, Allara D L, Tour J M and Weiss P S 2001 *Science* **292** 2303
[65] Fan F F, Yang J G, Dirk S M, Price D W, Kosynkin D, Tour J M and Bard A J 2001 *J. Am. Chem. Soc.* **213** 2454
[66] Chen J and Reed M A 2002 *Chem. Phys.* **281** 127
[67] Xue Y, Datta S, Hong S, Reifenberg R, Henderson J I and Kubiak C P 1999 *Phys. Rev.* B **59** R7852
[68] Xue Y, Datta S, Tian W, Hong S, Reifenberger R, Henderson J J and Kubiak C P 1999 *Phys. Rev.* B **59** 7852
[69] Hong S, Reifenberger R, Tian W, Datta S, Henderson J and Kubiak C P 2000 *Superlat. Microstruct.* **28** 289
[70] Joachim C, Gimzewski J K, Schlittler R R and Chavy C 1995 *Phys. Rev. Lett.* **74** 2102
[71] Joachim C and Gimzewski J K 1997 *Chem. Phys. Lett.* **265** 353
[72] Joachim C and Gimzewski J 1998 *Proc. IEEE* **86** 184
[73] Gimzewski J K and Joachim C 1999 *Science* **283** 1683
[74] Langlais V J, Schlittler R R, Tang H, Gourdon A, Joachim C and Gimzewski J K 1999 *Phys. Rev. Lett.* **83** 2809
[75] Joachim C, Gimzewski J K and Aviram A 2000 *Nature* **408** 541

[76] Rampi M A, Schueller O J and Whitesides G M 1998 *Appl. Phys. Lett.* **72** 1781
[77] Haag R, Rampi M A, Holmlin R E and Whitesides G M 1999 *J. Am. Chem. Soc.* **103** 7895
[78] Holmlin R E, Haag R, Ismagilov R F, Mujica V, Ratner M A, Rampi M A and Whitesides G M 2001 *Angew. Chem. Int. Ed. Engl.* **40** 2316
[79] Rampi M A and Whitesides G M 2002 *Chem. Phys.* **281** 373
[80] Tans S J, Devoret M H, Dai H, Thess A, Smalley R E, Geerligs L J and Dekker C 1997 *Nature* **386** 474
[81] Bezryadin A and Dekker C 1997 *J. Vac. Sci. Technol.* A **15** 793
[82] Dekker C 1999 *Phys. Today* **52** 22
[83] Porath D, Bezryadin A, de Vries S and Dekker C 2000 *Nature* **403** 635
[84] Metzger R M, Chen B, Höpfner U, Lakshmikantham M V, Vuillaume D, Kawai T, Wu X, Tachibana H, Hughes T V, Sakurai H, Baldwin J W, Hosch C, Cava M P, Brehmer L and Ashwell G J 1997 *J. Am. Chem. Soc.* **119** 10455
[85] Metzger R M, Chen B and Cava M P 1998 *Thin Solid Films* **327/329** 326
[86] For a review see,
Metzger R M 1999 *Acc. Chem. Res.* **32** 950
[87] Metzger R M, Xu T and Petersen I 2001 *J. Chem. Phys.* **105** 7280
[88] Wold D J and Frisbie C D 2000 *J. Am. Chem. Soc.* **122** 2970
[89] Wold D J and Frisbie C D 2001 *J. Am. Chem. Soc.* **123** 5549
[90] Dorogi M, Gomez J, Osifchin R, Andres R P and Reifenberger R 1995 *Phys. Rev.* B **52** 9071
[91] Fisher C M, Burghard M, Roth S and Klitzing K v 1995 *Appl. Phys. Lett.* **66** 3331
[92] Ebbesen T W, Lezec H J, Hiura H, Bennett J W, Ghaemi H F and Thio T 1996 *Nature* **382** 54
[93] Porath D, Levi Y, Tarabiah M and Millo O 1997 *Phys. Rev.* B **56** 9829
[94] Dhirani A-A, Lin P H, Guyot-Sionnest P, Zehner R W and Sita L R 1997 *J. Chem. Phys.* **106** 5249
[95] Kergueris C, Bourgoin J P and Palacin S 1999 *Nanotechnology* **10** 8
[96] Kergueris C, Bourgoin J P, Palacin S, Esteve D, Urbina C, Magoga M and Joachim C 1999 *Phys. Rev.* B **59** 12505
[97] Collier C P, Wong E W, Belohradsky M, Raymo F M, Stoddart J F, Kuekes P J, Williams R S and Heath J R 1999 *Science* **285** 391
[98] Slowinski K, Fong H K Y and Majda M 1999 *J. Am. Chem. Soc.* **103** 7257
[99] Collier C P, Mattersteig G, Wong E W, Luo Y, Beverly K, Sampaio J, Raymo F M, Stoddart J F and Heath J R 2000 *Science* **289** 1172
[100] Collet J, Lenfant S, Vuillaume D, Bouloussa O, Rondelez F, Gay J M, Kham K and Chevrot C 2000 *Appl. Phys. Lett.* **76** 1339
[101] Cui X D, Primak A, Zarate X, Tomfohr J, Sankey O F, Moore A L, Moore T A, Gust D, Harris G and Lindsay S M 2001 *Science* **294** 571
[102] Agrait N, Untiedt C, Rubio-Bollinger G and Vieira S 2002 *Chem. Phys.* **281** 231
[103] Patrone L, Palacin S, Bourgoin J P, Lagoute J, Zambelli T and Gauthier S 2002 *Chem. Phys.* **281** 325
[104] Weber H B, Reichert J, Weigend F, Ochs R, Beckmann D, Mayor M, Ahlrichs R and Löhneysen H v 2002 *Chem. Phys.* **281** 113
[105] Alavi S and Seideman T 2001 *J. Chem. Phys.* **115** 1882
[106] Alavi S, Larade B, Taylor J, Guo H and Seideman T 2002 *Chem. Phys.* **281** 293
[107] Alavi S, Rousseau R and Seideman T 2000 *J. Chem. Phys.* **113** 4412
[108] Alavi S, Rousseau R, Patitsas S N, Lopinski G P, Wolkow R A and Seideman T 2000 *Phys. Rev. Lett.* **85** 5372
[109] Alavi S, Rousseau R, Lopinski G P, Wolkow R A and Seideman T 2000 *Faraday Discuss.* **117** 213
[110] Domcke W and Cederbaum L S 1977 *J. Phys. B: At. Mol. Phys.* **10** L47
[111] For a review see,
Guo H, Saalfrank P and Seideman T 1999 *Prog. Surf. Sci.* **62** 239
[112] For a review see,
Gadzuk J W 1988 *Annu. Rev. Phys. Chem.* **39** 395
[113] Almbladh C O and Minnhagen P 1978 *Phys. Rev.* B **17** 929
[114] Gadzuk J W 1991 *Phys. Rev.* B **44** 13466
[115] See, for instance,
Berlin Y A, Burin A L and Ratner M A 2002 *Chem. Phys.* **275** 61 and references therein
[116] Gao S, Persson M and Lundqvist B I 1997 *Phys. Rev.* B **55** 4825
[117] Persson B N J and Baratoff A 1987 *Phys. Rev. Lett.* **59** 339
[118] Gata M A and Antoniewicz P R 1993 *Phys. Rev.* B **47** 13797
[119] Levine R D 1969 *Quantum Mechanics of Molecular Rate Processes* (Oxford: Oxford University Press)
[120] Lu P H, Polanyi J C and Rogers D 2000 *J. Chem. Phys.* **112** 11005

[121] Wallis T M, Chen X and Ho W 2000 *J. Chem. Phys.* **113** 4837
[122] Lauhon L J and Ho W 2000 *Faraday Discuss.* **117** 249
[123] Lauhon L J and Ho W 2001 *Rev. Sci. Instrum.* **72** 26
[124] Lorente N, Persson M, Lauhon L J and Ho W 2001 *Phys. Rev. Lett.* **86** 2593
[125] Gaudioso J and Ho W 2001 *J. Am. Chem. Soc.* **123** 10095
[126] Foley E T, Kam A F, Lyding J W and Avouris Ph 1998 *Phys. Rev. Lett.* **80** 1336
[127] Bartels L, Meyer G, Rieder K-H, Velic D, Knoesel E, Hotzel A, Wolf M and Ertl G 1998 *Phys. Rev. Lett.* **80** 2004
[128] Stipe B C, Rezaei M A and Ho W 1998 *Phys. Rev. Lett.* **81** 1263
[129] Lauhon L J and Ho W 2000 *Surf. Sci.* **451** 219
[130] Stipe B C, Rezaei M A and Ho W 1997 *Phys. Rev. Lett.* **79** 4397
[131] See, for instance,
Lorente N and Persson M 2000 *Faraday Discuss.* **117** 277
[132] See, for instance,
Levine R D 1969 *Quantum Mechanics of Molecular Rate Processes* (Oxford: Oxford University Press) section 3.3.0
[133] Goldberger M L and Watson K M 1964 *Phys. Rev.* B **136** 1472
[134] Miller W H 1998 *J. Phys. Chem.* A **102** 793 and references therein
[135] Menzel D and Gomer R 1964 *J. Chem. Phys.* **41** 3311
Redhead P A 1964 *Can. J. Phys.* **64** 886
[136] Gadzuk J W 1995 *Surf. Sci.* **342** 345
[137] Avouris Ph, Walkup R E, Rossi A R, Akpati H C, Nordlander P, Shen T-C, Abeln G C and Lyding J W 1996 *Surf. Sci.* **363** 368
[138] Lyding J W, Shen T-C, Hubacek J S, Tucker J R and Abeln G C 1994 *Appl. Phys. Lett.* **64** 2010
[139] Adams D P, Mayer T M and Swartzentruber B S 1996 *J. Vac. Sci. Technol.* B **14** 1642
[140] Hersam M C, Guisinger N P and Lyding J W 2000 *Nanotechnology* **11** 70
[141] Maruno S, Iwasaki H, Horioka K, Li S-T and Nakamura S 1983 *Phys. Rev.* B **27** 4110
[142] Shen T-C, Wang C, Abeln G C, Tucker J R, Lyding J W, Avouris Ph and Walkup R E 1995 *Science* **268** 1590
[143] Ciraci S, Butz R, Oelig E M and Wagner H 1984 *Phys. Rev.* B **30** 711
[144] Vondrak T and Zhu X-Y 1999 *J. Phys. Chem.* B **103** 4892
Vondrak T and Zhu X-Y 1999 *Phys. Rev. Lett.* **82** 1967
[145] Avouris Ph, Walkup R E, Rossi A R, Shen T-C, Abeln G C, Tucker J R and Lyding J W 1996 *Chem. Phys. Lett.* **257** 148
Shen T-C and Avouris Ph 1997 *Surf. Sci.* **390** 35
[146] Chelikowsky J R and Cohen M L 1976 *Phys. Rev.* B **556**
[147] Chen C J 1988 *J. Vac. Sci. Technol.* A **6** 319
[148] Ohnishi S and Tsukada M 1989 *Solid State Commun.* **71** 391
[149] Doyen G, Koetter E, Vigneron J P and Scheffler M 1990 *Appl. Phys.* A **51** 281
[150] Hofer W A and Redinger J 2000 *Surf. Sci.* **447** 51
[151] Levy Yeyati A, Martín-Rodero A and Flores F 1997 *Phys. Rev.* B **56** 10369
[152] Vázquez de Parga A L, Hernán O S, Miranda R, Levy Yeyati A, Mingo N, Martín-Rodero A and Flores F 1998 *Phys. Rev. Lett.* **80** 357
[153] Gokhale S, Trischberger P, Menzel D, Widdra W, Dröge H, Steinrück H-P, Birkenheuer U, Gutdeutsch U and Rösch N 1998 *J. Chem. Phys.* **108** 5554
[154] Guo H and Seideman T 1995 *J. Chem. Phys.* **103** 9062
[155] Park H, Park J, Lim A K L, Anderson E H, Alivisatos A P and McEuen P L 2000 *Nature* **407** 57
[156] Chavy C, Joachim C and Altibelli A 1993 *Chem. Phys. Lett.* **214** 569
[157] For a review see,
Balzani V, Credi A, Raymo F M and Stoddart J F 1998 *Angew. Chem. Int. Ed.* **39** 3348
[158] Huang Y, Rettner C T, Auerbach D J and Wodtke A M 2000 *Science* **290** 111
[159] Wolkow R A 1999 *Annu. Rev. Phys. Chem.* **50** 413
[160] Hamers R J, Coulter S K, Ellison M D, Hovis J S, Padowitz D F, Schwartz M P, Greenlief C M and Russell J N Jr 2000 *Acc. Chem. Res.* **33** 617